The Atmospheric Boundary Layer Over Polar Marine Surfaces

Edgar L Andreas

June 1996

Unstable Boundary Layer

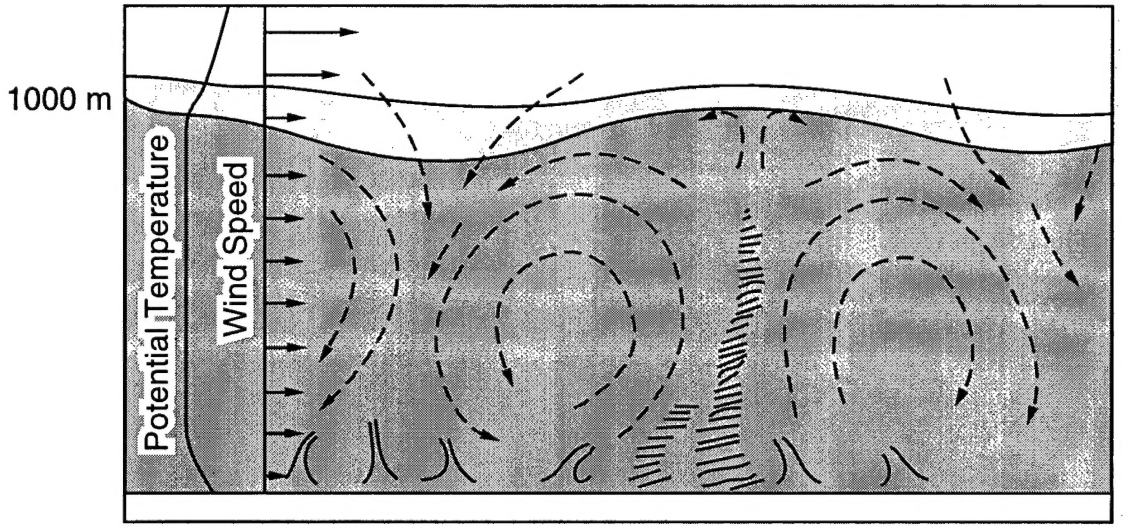

Stable Boundary Layer

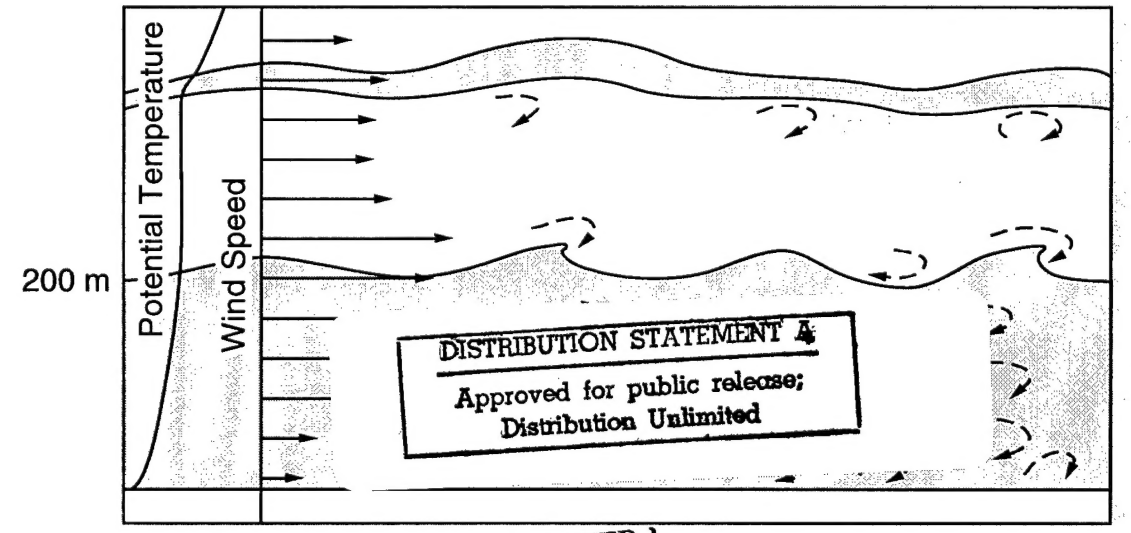

Abstract: The Atmospheric Boundary Layer (ABL) over polar marine surfaces is, in ways, simpler and, in other ways, more complex than ABLs in other environments. It is simpler because topographic effects are rarely a concern, the surface is fairly homogeneous, and roughness lengths over sea ice and the ocean are much smaller than they are over land. It is complex because the stratification is usually stable, and stable ABLs have not yielded to quantification as readily as convective ABLs have. This report reviews some of these characteristics of ABLs over polar marine surfaces. The ABL, by definition, is the turbulent layer between the Earth's surface and the (generally) nonturbulent free atmosphere. Hence, the emphasis is on turbulence processes—in particular, the turbulent transfer of momentum and sensible and latent heat over sea ice. As such, this report reviews both the theoretical and observational bases for our understanding of the mean structure of the ABL. Understanding this structure then allows predicting the turbulent surface fluxes of momentum and sensible and latent heat.

Cover: Schematic depictions of unstable (or convective) and stable atmospheric boundary layers. The unstable boundary layer is characterized by large eddies, convective plumes, a capping version, and well mixed (i.e., constant) profiles of wind speed and potential temperature. The stable boundary layer is shallower and has smaller eddies and steeper vertical gradients in wind speed and potential temperature. The density gradient through the inversion may allow gravity waves to exist at the top of the boundary layer; there also may be a low-level jet resulting from inertial oscillations and intermittent turbulence near the inversion (adapted from Wyngaard 1992).

How to get copies of CRREL technical publications:

Department of Defense personnel and contractors may order reports through the Defense Technical Information Center:

DTIC-BR SUITE 0944
8725 JOHN J KINGMAN RD
FT BELVOIR VA 22060-6218
Telephone 1 800 225 3842
E-mail help@dtic.mil
msorders@dtic.mil
WWW http://www.dtic.dla.mil/

All others may order reports through the National Technical Information Service:

NTIS
5285 PORT ROYAL RD
SPRINGFIELD VA 22161
Telephone 1 703 487 4650
1 703 487 4639 (TDD for the hearing-impaired)
E-mail orders@ntis.fedworld.gov
WWW http://www.fedworld.gov/ntis/ntishome.html

A complete list of all CRREL technical publications is available from:

USACRREL (CECRL-TL)
72 LYME RD
HANOVER NH 03755-1290
Telephone 1 603 646 4338
E-mail techpubs@crrel.usace.army.mil

For information on all aspects of the Cold Regions Research and Engineering Laboratory, visit our World Wide Web site:
http://www.crrel.usace.army.mil

Monograph 96-2

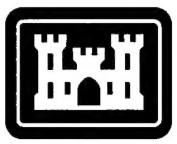

US Army Corps of Engineers
Cold Regions Research & Engineering Laboratory

The Atmospheric Boundary Layer Over Polar Marine Surfaces

Edgar L Andreas

June 1996

PREFACE

This report was prepared by Dr. Edgar L Andreas, Research Physicist, Snow and Ice Division, Research and Engineering Directorate, U.S. Army Cold Regions Research and Engineering Laboratory.

The author thanks Kerry Claffey for help with the Ice Station Weddell (ISW) observations; his Ice Station Weddell colleagues Aleksandr Makshtas and Boris Ivanov for their conscientious airborne snow observations, which yielded Figure 14; Alfred Blackadar for allowing reproduction of Figure 24; Rachel Jordan and Peter Guest, who offered helpful comments on the manuscript; Mark Hardenberg for editorial assistance; the U.S. National Science Foundation, which supported this work through grants OPP-90-24544 and OPP-93-12642; the Office of Naval Research, which supported it with contract N0001496MP30005; and the U.S. Department of the Army, which supported it through project 4A161102AT24.

CONTENTS

ILLUSTRATIONS

Figure

Figure

TABLES

Table

The Atmospheric Boundary Layer Over Polar Marine Surfaces

EDGAR L ANDREAS

INTRODUCTION

The Atmospheric Boundary Layer (ABL) is the lowest few hundred meters of the atmosphere, where the Earth's surface most directly influences atmospheric processes. The vast majority of Earth's human inhabitants are never outside the ABL.

I cannot hope, in a few pages here, to compete with the many good books recently published on the ABL (Arya 1988, Stull 1988, Sorbjan 1989, Garratt 1992, Kaimal and Finnigan 1994)—nor do I need to. My purpose here is to present some of the basic concepts of boundary-layer meteorology, to define some of the jargon a relative novice might encounter in the above (and other) texts, and to describe a few of the unique problems associated with the ABL over polar marine surfaces.

This report divides into two logical parts. In the first part, I focus on microscale processes in the so-called Atmospheric Surface Layer (ASL). The height scale relevant in the ASL is generally 10–30 m; relevant horizontal scales are a few hundred meters. In the second part, I tie surface-layer processes to the structure of the entire ABL. Here, the relevant height scale is the height of the ABL—typically a few hundred meters over polar marine surfaces. The relevant horizontal scale is on the order of kilometers.

BASIC EQUATIONS OF AN ICE FLOE

The momentum balance of a floating ice floe is (e.g., Hibler 1979)

$$m\frac{D\bar{u}}{Dt} = \bar{\tau} - \bar{\tau}_w + mf\bar{k}\times\bar{u} - mg\vec{\nabla}H + \bar{I}. \qquad (1)$$

Here, m is the mass of the floe; $\bar{u}$ is the velocity vector of the floe; D/Dt is the material derivative

$$\frac{D}{Dt} = \frac{\partial}{\partial t} + \bar{u}\cdot\vec{\nabla} \qquad (2)$$

where $\bar{\tau}$ = vectoral stress exerted on the top of the floe by the wind
$\bar{\tau}_w$ = vectoral stress exerted on the underside of the floe by the water
f = Coriolis parameter
$\bar{k}$ = vertical unit vector
$\vec{\nabla}H$ = gradient in sea surface height
$\bar{I}$ = internal ice forces vector.

$\bar{\tau}$ and $\bar{\tau}_w$ are the only turbulence terms in eq 1. Thus, the main concern boundary-layer meteorologists have with eq 1 is evaluating $\bar{\tau}$, the surface stress on the top side of the ice. The desire to know $\bar{\tau}$ motivates much of what I will write in this monograph.

The energy budget at the surface of an ice floe is (e.g., Maykut 1978, Parkinson and Washington 1979, Makshtas 1991)

$$B = Q_s - \alpha_s Q_s + Q_{L\downarrow} - Q_{L\uparrow} - H_s - H_L + C \qquad (3a)$$

$$= \text{melting/freezing} + \text{storage/release}. \qquad (3b)$$

Here Q_s = incoming shortwave radiation
α_s = shortwave albedo
$\alpha_s Q_s$ = reflected shortwave radiation
$Q_{L\downarrow}$ = incoming longwave radiation
$Q_{L\uparrow}$ = emitted longwave radiation
C = conduction to the ice surface from below
H_s = turbulent sensible heat flux (the flux driven by a difference in temperature between the ice surface and the air)
H_L = turbulent latent heat flux (the flux driven by a difference in water vapor density between the surface and the air).

In eq 3, my convention is that positive terms add heat to the ice surface; negative terms carry heat away. Thus, for example, when H_s and H_L are positive, turbulence is carrying heat from the surface into the air.

If the seven terms on the right-hand side of eq 3a do

not add to zero, the energy balance B is nonzero. As a result, this energy imbalance must reflect phase changes (freezing or melting) or warming or cooling (storage or release of heat) of the ice within the floe.

As a boundary-layer meteorologist, I could justifiably study any but the C term on the right-hand side of eq 3a. But since my main interest is turbulence in the ABL, I will confine my attention here to H_s and H_L. These are the only two turbulence terms in eq 3. As I said for $\bar{\tau}$, the desire to know H_s and H_L is the basis for most of what I will write here.

THE NAVIER-STOKES EQUATION

All geophysical fluid dynamics starts with the Navier-Stokes equation (e.g., Busch 1973, Businger 1982)

$$\underset{\text{I}}{\frac{\partial \tilde{u}_i}{\partial t}} + \underset{\text{II}}{\tilde{u}_j \frac{\partial \tilde{u}_i}{\partial x_j}} = \underset{\text{III}}{-\frac{1}{\tilde{\rho}} \frac{\partial \tilde{p}}{\partial x_i}} \underset{\text{IV}}{- g\delta_{i3}} \underset{\text{V}}{- 2\Omega\varepsilon_{ijk}\eta_j \tilde{u}_k} + \underset{\text{VI}}{\nu \frac{\partial^2 \tilde{u}_i}{\partial x_j \partial x_j}}. \tag{4}$$

In my notation, a wavy overbar indicates an instantaneous value; $\tilde{u}_i$, for example, is the i^{th} component of the instantaneous fluid velocity vector. Thus, eq 4 shows the processes that affect this component.

In eq 4, term I is the time rate of change (the acceleration) of the i^{th} component. Term II really contains three terms since the repeated j index indicates a sum. It shows the advective effects on the i^{th} velocity component. In term III, $\tilde{\rho}$ is fluid density and $\tilde{p}$ is the pressure. Term III, thus, shows the effects of a pressure gradient on the fluid—fluid tends to accelerate down the gradient. In term IV, g is the acceleration of gravity, and δ_{ij} is the Kronecker delta, where $\delta_{ij} = 1$ if $i = j$, and $\delta_{ij} = 0$ if $i \neq j$. Term IV therefore represents the gravitational force and affects only the $\tilde{u}_3$ component of the velocity (the vertical component). Term V shows the Coriolis effects on the fluid motion. Here Ω is the Earth's rotation rate, 2π radians per day (7.27×10^{-5} s^{-1}), and η_j is the unit vector of the Earth's rotational axis

$$\bar{\eta} = (0, \cos\lambda, \sin\lambda) \tag{5}$$

where λ is the latitude. Notice, the quantity f in eq 1 is

$$f = 2\Omega \sin\lambda\,. \tag{6}$$

Finally, term VI quantifies viscous effects on the flow, where ν is the kinematic viscosity of the fluid.

We can write an equation analogous to eq 4 for the conservation of any conservative scalar—potential temperature $\tilde{\theta}$, for example (Busch 1973, Businger 1982)

$$\underset{\text{I}}{\frac{\partial \tilde{\theta}}{\partial t}} + \underset{\text{II}}{\tilde{u}_j \frac{\partial \tilde{\theta}}{\partial x_j}} = \underset{\text{III}}{D \frac{\partial^2 \tilde{\theta}}{\partial x_j \partial x_j}}. \tag{7}$$

Here, term I is the time rate of change of the instantaneous temperature. Term II quantifies advective effects on the temperature. Term III contains the molecular effects on the temperature, where D is the thermal diffusivity of heat in the fluid.

In the atmosphere, the instantaneous specific humidity $\tilde{q}$ is usually another conservative scalar. We can write an equation for it with exactly the same form as eq 7

$$\frac{\partial \tilde{q}}{\partial t} + \tilde{u}_j \frac{\partial \tilde{q}}{\partial x_j} = D_w \frac{\partial^2 \tilde{q}}{\partial x_j \partial x_j} \tag{8}$$

where D_w is the molecular diffusivity of water vapor in air.

Equation 4, especially, is too complex to treat as it stands; we need to simplify it. Our first simplification is to recognize that each instantaneous quantity in eq 4, 7 and 8 can be decomposed into an average and a turbulent fluctuation about that average. That is,

$$\tilde{u}_i = U_i + u_i \tag{9a}$$

$$\tilde{\theta} = \Theta + \theta \tag{9b}$$

$$\tilde{q} = Q + q \tag{9c}$$

$$\tilde{\rho} = \rho_0 + \rho \tag{9d}$$

$$\tilde{p} = P + p. \tag{9e}$$

In eq 9, a capital letter indicates an averaged quantity, except in eq 9d where ρ_0 indicates the average air density. A lower case letter without the wavy overbar is a zero-mean turbulent fluctuation about that average.

Let me demonstrate how to manipulate these decomposed quantities. Let a straight overbar indicate averaging. Then, with $\tilde{u}_i$ for example

$$\overline{\tilde{u}_i} = U_i \tag{10}$$

since the average of u_i is zero by definition ($\overline{u_i} \equiv 0$). Similarly

$$\overline{\tilde{u}_i \tilde{u}_j} = \overline{(U_i + u_i)(U_j + u_j)} \tag{11a}$$

$$= \overline{U_i U_j} + \overline{u_i U_j} + \overline{u_j U_i} + \overline{u_i u_j} \tag{11b}$$

$$= U_i U_j + \overline{u_i u_j} \tag{11c}$$

since U_i and U_j are already averaged quantities.

I could digress here and spend 10–20 pages discussing what the averaging denoted by that straight overbar means. Ideally, it denotes an ensemble average (Lumley and Panofsky 1964, p. 6)—the average formed from data collected during repeated, identical experiments. In the atmospheric sciences, however, we do not have the luxury of ensemble averaging. To create averages, we must make an ergodic hypothesis (Lumley and Panofsky 1964, p. 35)—that conditions are near enough to steady state that a time average is equivalent to an ensemble average. Lumley and Panofsky (1964, p. 35 ff.), Haugen et al. (1971), Wyngaard (1973) and Andreas (1988), among others, have considered what the appropriate averaging time is for ABL statistics. In light of these studies, henceforth in this report I will use upper-case variables to mean averages obtained from an hour's worth of instantaneous values. Likewise, the straight overbar, in $\overline{u_i u_j}$ for example, will mean a turbulence statistic obtained by averaging for 1 hour. Notice that, because these are time averages not volume averages, an averaged quantity may still depend on position within the fluid.

To write eq 4, 7 and 8, we have already made some approximations. To simplify these further, we will make additional approximations. These are the Boussinesq approximations (Busch 1973; Businger 1982; Garratt 1992, p. 20 f.), which I summarize here.

The Boussinesq Approximations

1. The dynamic viscosity, $\mu = \rho_0 \nu$; the thermal conductivity of air, $k_T = \rho_0 c_p D$, where c_p is the specific heat of air at constant pressure; and D_w are constants throughout the fluid.
2. The flow speeds are low enough that the air behaves as an incompressible fluid.
3. Turbulent fluctuations in fluid properties are much smaller than the corresponding averages; that is $\theta/\Theta \ll 1$, $q/Q \ll 1$, $\rho/\rho_0 \ll 1$ and $p/P \ll 1$.
4. p/P can be neglected in comparison to θ/Θ, q/Q and ρ/ρ_0.
5. The heat generated by viscous stresses can be neglected. In other words, term VI in eq 4 does not need to appear as a source term in eq 7.
6. Turbulent density fluctuations, ρ, are significant only when they multiply g.

Now back to the Navier-Stokes equation, eq 4. Substitute in it eq 9a, 9d and 9e, then average. The result is

$$\frac{\partial U_i}{\partial t} + U_j \frac{\partial U_i}{\partial x_j} + \frac{\partial}{\partial x_j} \overline{u_i u_j} = \frac{1}{\rho_0} \frac{\partial P}{\partial x_i} - g \delta_{i3} - 2\Omega \varepsilon_{ijk} \eta_j U_k + \nu \frac{\partial^2 U_i}{\partial x_j \partial x_j}. \qquad (12)$$

The second and third terms on the left-hand side derive from the assumption that the atmosphere is incompressible

$$\frac{\partial U_j}{\partial x_j} = 0 \qquad (13a)$$

$$\frac{\partial u_j}{\partial x_j} = 0. \qquad (13b)$$

The first term on the right-hand side of eq 12 is a consequence of another of the Boussinesq approximations—that fluctuations in fluid density are much less than the mean density and, therefore, only important when they multiply g.

In horizontally homogeneous conditions, the x (or x_1) and y (or x_2) derivatives in eq 12 produce zeroes, except in $\partial P/\partial x$ and $\partial P/\partial y$, which are imposed synoptic-scale forcings. Near an impermeable surface, such as sea ice or the ocean, the average vertical velocity, W (or U_3), must be zero. Lastly, the viscous term in eq 12 is always small except within a few millimeters of the surface. Hence, in an ABL above a horizontally homogeneous surface, the three equations implicit in eq 12 become

U equation

$$\frac{\partial U}{\partial t} = -\frac{\partial \overline{uw}}{\partial z} - \frac{1}{\rho_0} \frac{\partial P}{\partial x} + f V \qquad (14a)$$

V equation

$$\frac{\partial V}{\partial t} = -\frac{\partial \overline{vw}}{\partial z} - \frac{1}{\rho_0} \frac{\partial P}{\partial y} - f U \qquad (14b)$$

W equation

$$g = -\frac{1}{\rho_0} \frac{\partial P}{\partial z}. \qquad (14c)$$

The W equation, which results from the assumption that vertical accelerations are much less than pressure gradient forces (Pielke 1984, p. 30 ff.), shows that, on average, the ABL is in hydrostatic balance.

In eq 14a and b, it is common to substitute the geostrophic wind components U_g and V_g, defined as

$$fV_g \equiv \frac{1}{\rho_0}\frac{\partial P}{\partial x} \tag{15a}$$

$$-fU_g \equiv \frac{1}{\rho_0}\frac{\partial P}{\partial y}. \tag{15b}$$

Thus, eq 14a and b become

$$\frac{\partial U}{\partial t} = -\frac{\partial \overline{uw}}{\partial z} + f\left(V - V_g\right) \tag{16a}$$

$$\frac{\partial V}{\partial t} = -\frac{\partial \overline{vw}}{\partial z} - f\left(U - U_g\right). \tag{16b}$$

The $\partial\overline{uw}$ and $\partial\overline{vw}$ terms in eq 16 really contain the essence of what we mean by an atmospheric boundary layer. Without these terms, and assuming for the moment steady-state conditions, eq 16 would reduce to a simple geostrophic balance characterized by two-dimensional flow. Such conditions are common in the free atmosphere, but the ABL is by definition a turbulent layer, and turbulence by definition is three-dimensional. The $\partial\overline{uw}$ and $\partial\overline{vw}$ terms in eq 16, thus, give the ABL its character.

For the atmosphere, the ideal gas law is the appropriate equation of state (Lumley and Panofsky 1964, p. 214)

$$\tilde{p} = R\tilde{\rho}\tilde{t}_v. \tag{17}$$

Here R (= 287.056 J kg^{-1} K^{-1}) is the universal gas constant for dry air, and $\tilde{t}_v$ is the instantaneous virtual temperature, a temperature that reflects the fact that the presence of water vapor affects air density.

As usual

$$\tilde{t}_v = T_v + t_v. \tag{18}$$

Lumley and Panofsky (1964, p. 213 f.) showed that

$$\tilde{t}_v = \tilde{t}_a\left[1 + \left(\frac{M_a}{M_w} - 1\right)\tilde{q}\right] \tag{19a}$$

$$= \tilde{t}_a\left(1 + 0.61\tilde{q}\right) \tag{19b}$$

where M_a (= 28.9644 × 10^{-3} kg/mol) is the molecular weight of dry air, and M_w (= 18.0160 × 10^{-3} kg/mol) is the molecular weight of water. Here, also, $\tilde{t}_a$ is the instantaneous air temperature

$$\tilde{t}_a = T + \theta \tag{20}$$

where T is the average air temperature. In eq 20, we also use the fact that the turbulent fluctuations in potential temperature and in air temperature are virtually identical. From eq 19b, 18, 9c and 20, we see that, to a good approximation

$$T_v = T(1 + 0.61Q) \tag{21a}$$

$$t_v = \theta(1 + 0.61Q) + 0.61Tq. \tag{21b}$$

Expanding eq 17, we get

$$P + p = R\rho_0 T_v\left(1 + \frac{\rho}{\rho_0} + \frac{t_v}{T_v} + \frac{\rho}{\rho_0}\frac{t_v}{T_v}\right). \tag{22}$$

On ignoring the fourth term on the right-hand side of eq 22, because it is much smaller than the other terms, then averaging, we get the mean equation of state

$$P = R\rho_0 T_v. \tag{23}$$

On subtracting this from eq 22, we find

$$\frac{p}{R\rho_0 T_v} = \frac{p}{P} = \frac{\rho}{\rho_0} + \frac{t_v}{T_v}. \tag{24}$$

According to the Boussinesq approximations, however, the left side of this equation is negligible in comparison to the right side. Consequently, the equation of state for the fluctuating quantities is

$$\frac{\rho}{\rho_0} = -\frac{t_v}{T_v}. \tag{25}$$

In eq 4, let us look at term III with this equation of state in mind. We have

$$\frac{1}{\tilde{\rho}}\frac{\partial \tilde{p}}{\partial x_i} = \frac{1}{\rho_0 + \rho}\frac{\partial\left(P + p\right)}{\partial x_i}. \tag{26}$$

After some simple manipulations, this becomes

$$\frac{1}{\tilde{\rho}}\frac{\partial \tilde{p}}{\partial x_i} = \frac{1}{\rho_0}\frac{\partial P}{\partial x_i} + \frac{1}{\rho_0}\frac{\partial p}{\partial x_i} - \frac{\rho}{\rho_0^2}\frac{\partial P}{\partial x_i} - \frac{\rho}{\rho_0^2}\frac{\partial p}{\partial x_i}. \tag{27}$$

Again, the fourth term on the right is much smaller than the others; we ignore it. According to the Boussinesq approximation, the density fluctuation in the third term on the right is important only when it multiplies the acceleration of gravity. Thus, from eq 14c and 25, this term is

$$-\frac{\rho}{\rho_0^2}\frac{\partial P}{\partial x_i} = \frac{\rho g}{\rho_0}\delta_{i3} = -\frac{t_v g}{T_v}\delta_{i3}. \tag{28}$$

Consequently, term III in eq 4 is

$$\frac{1}{\tilde{\rho}}\frac{\partial \tilde{p}}{\partial x_i} = \frac{1}{\rho_0}\frac{\partial P}{\partial x_i} + \frac{1}{\rho_0}\frac{\partial p}{\partial x_i} - \frac{t_v\, g}{T_v}\delta_{i3}. \qquad (29)$$

With eq 29 substituted into eq 4, we subtract eq 12 to get an equation for the turbulent velocity component u_i

$$\frac{\partial u_i}{\partial t} + \frac{\partial}{\partial x_i}\left(U_i u_j + u_i U_j + u_i u_j - \overline{u_i u_j}\right)$$

$$= -\frac{1}{\rho_0}\frac{\partial p}{\partial x_i} + \frac{t_v\, g}{T_v}\delta_{i3} - 2\Omega\varepsilon_{ijk}\,\eta_j u_k + \nu\frac{\partial^2 u_i}{\partial x_j \partial x_j}. \qquad (30)$$

Multiply this equation by u_i, then average. After some manipulations, we get

$$\frac{\partial \overline{e^2}}{\partial t} = -\overline{u_i u_j}\frac{\partial U_i}{\partial x_j} - U_j\frac{\partial \overline{e^2}}{\partial x_j} - \frac{\partial \overline{e^2 u_j}}{\partial x_j} - \frac{1}{\rho_0}\frac{\partial \overline{u_i p}}{\partial x_j} + \frac{\overline{w t_v}\, g}{T_v}$$

$$-2\Omega\varepsilon_{ijk}\,\eta_j\,\overline{u_i u_k} - \nu\overline{\frac{\partial u_i}{\partial x_j}\frac{\partial u_i}{\partial x_j}} + \nu\frac{\partial^2 \overline{e^2}}{\partial x_j \partial x_j}. \qquad (31)$$

Here

$$e^2 \equiv \frac{1}{2}u_i u_i = \frac{1}{2}\left(u^2 + v^2 + w^2\right) \qquad (32)$$

and $\overline{e^2}$ is the average Turbulent Kinetic Energy (TKE).

In eq 31, we henceforth ignore the last term on the right-hand side, the viscous transport term, because it is small except very near the surface. The Coriolis term in eq 31 is identically zero because $\varepsilon_{ijk}u_i u_k = u_i u_k - u_k u_i$ for all j.

Again invoking horizontal homogeneity in an atmospheric surface layer (where $W = 0$) and assuming that the mean wind is in the x direction (i.e., $V = 0$), we finally derive the turbulent kinetic energy equation from eq 31

$$\frac{\partial \overline{e^2}}{\partial t} = \underbrace{-\overline{uw}\frac{\partial U}{\partial z}}_{\text{I}} \quad \underbrace{+\frac{g}{T_v}\overline{w t_v}}_{\text{II}} \quad \underbrace{-\frac{\partial}{\partial z}\left(\overline{we^2} + \frac{\overline{wp}}{\rho_0}\right)}_{\text{III}} \quad \underbrace{-\varepsilon}_{\text{IVa}} \quad \underbrace{}_{\text{IVb}} \quad \underbrace{}_{\text{V}} \qquad (33)$$

Here, term I is the time rate of change of TKE. Term II represents mechanical production of TKE; the Reynolds stresses (e.g., $\overline{uw}$) extract energy from the mean wind speed gradient. Term III is the buoyancy production of TKE. Term IV shows that TKE changes because of turbulent transport. Term IVa represents the vertical turbulent advection of TKE; term IVb represents a transport resulting from a correlation between the vertical velocity fluctuations and the pressure fluctuations. Term V, which is

$$\varepsilon \equiv \nu\overline{\frac{\partial u_i}{\partial x_j}\frac{\partial u_i}{\partial x_j}} \qquad (34)$$

is called the dissipation rate of TKE. Because in eq 34 $\partial u_i/\partial x_j$ is a squared quantity, ε is always positive. But since ε appears with a minus sign in eq 33, term V is always a sink for TKE. It represents the dissipation of the turbulence to heat because of viscous effects.

In summary, eq 33 shows the processes that are important in maintaining the turbulence in an atmospheric surface layer. For example, for steady-state conditions, the turbulent transport terms in eq 33 (IV) are often small. Consequently, mechanical (II) and buoyant (III) production nearly balance viscous dissipation (V). Production equals dissipation (Panofsky and Dutton 1984, p. 92 ff.; Fairall and Larsen 1986).

Starting with the scalar conservation equations, eq 7 and 8, we can follow a procedure similar to that above to derive equations for scalar means and variances. With potential temperature as an example, insert eq 9a and b into eq 7 and average. The result is

$$\frac{\partial \Theta}{\partial t} + U_j\frac{\partial \Theta}{\partial x_j} + \frac{\partial \overline{u_j\theta}}{\partial x_j} = D\frac{\partial^2 \Theta}{\partial x_j \partial x_j}. \qquad (35)$$

Now subtract eq 35 from eq 7 to get a conservation equation for the turbulent temperature fluctuations

$$\frac{\partial \theta}{\partial t} + u_j\frac{\partial \Theta}{\partial x_j} + U_j\frac{\partial \theta}{\partial x_j} + \frac{\partial u_j\theta}{\partial x_j} - \frac{\partial \overline{u_j\theta}}{\partial x_j} = D\frac{\partial^2 \theta}{\partial x_j \partial x_j}. \qquad (36)$$

Multiply this equation by θ and average

$$\frac{\partial \overline{\theta^2}}{\partial t} = -2\overline{u_j\theta}\frac{\partial \Theta}{\partial x_j} - U_j\frac{\partial \overline{\theta^2}}{\partial x_j} - \frac{\partial^2 \overline{u_j\theta^2}}{\partial x_j}$$

$$-2D\overline{\frac{\partial \theta}{\partial x_j}\frac{\partial \theta}{\partial x_j}} + D\frac{\partial^2 \overline{\theta^2}}{\partial x_j \partial x_j}. \qquad (37)$$

As in eq 31, we can ignore the molecular transport term, the last term in eq 37. Again assume horizontal homogeneity, that we are within a few tens of meters of the surface (so $W = 0$), and that x is in the direction of the mean wind vector (i.e., $V = 0$). With these simplifications, the mean equation for potential temperature becomes

$$\frac{\partial \Theta}{\partial t} + \frac{\partial \overline{w\theta}}{\partial z} = D\frac{\partial^2 \Theta}{\partial z^2} \qquad (38)$$

and the conservation equation for temperature variance is

$$\underset{\text{I}}{\frac{\partial\overline{\theta^2}}{\partial t}} = \underset{\text{II}}{-2\overline{w\theta}\frac{\partial\Theta}{\partial z}} \underset{\text{III}}{-\frac{\partial\overline{w\theta^2}}{\partial z}} \underset{\text{IV}}{-N_\theta}. \tag{39}$$

In eq 39, term I is the time rate of change of temperature variance. Term II is the production of temperature variance through the interaction of the vertical temperature flux ($\overline{w\theta}$) with the mean temperature gradient. Term III is the turbulent transport of temperature variance by the vertical velocity fluctuations. Term IV, which by definition is

$$N_\theta \equiv 2D\overline{\frac{\partial\theta}{\partial x_j}\frac{\partial\theta}{\partial x_j}} \tag{40}$$

is always positive. Since it appears with a minus sign in eq 39, in analogy with ε, it represents the rate at which molecular processes dissipate the temperature variance.

From the conservation equation for specific humidity, eq 8, we can follow exactly the same procedure as above for potential temperature to derive conservation equations for the mean specific humidity

$$\frac{\partial Q}{\partial t} + \frac{\partial\overline{wq}}{\partial z} = D_w\frac{\partial^2 Q}{\partial z^2} \tag{41}$$

and for the humidity variance

$$\frac{\partial\overline{q^2}}{\partial t} = -2\overline{wq}\frac{\partial Q}{\partial z} - \frac{\partial\overline{wq^2}}{\partial z} - N_q \tag{42}$$

where

$$N_q \equiv 2D_w\overline{\frac{\partial q}{\partial x_j}\frac{\partial q}{\partial x_j}} \tag{43}$$

is the dissipation rate of specific humidity variance.

As in the TKE equation, eq 33, it is common in eq 39 and 42 to assume steady state and that the turbulent transport terms are small. Production then again equals dissipation (Large and Pond 1982; Panofsky and Dutton 1984, p. 94).

MONIN-OBUKHOV SIMILARITY

The equations for the mean velocity components, eq 16, the mean potential temperature, eq 38, and the mean specific humidity, eq 41, provide some important insights into processes in the atmospheric surface layer.

Let me define nondimensional versions (denoted by +) of the variables in eq 16 that are appropriate in an ASL

$$U_+ = U/G \tag{44a}$$

$$V_+ = V/G \tag{44b}$$

$$U_{g+} = U_g/G \tag{44c}$$

$$V_{g+} = V_g/G \tag{44d}$$

$$t_+ = f\,t \tag{44e}$$

$$z_+ = z/z_0. \tag{44f}$$

Here

$$G = \left(U_g^2 + V_g^2\right)^{1/2} \tag{45}$$

is the magnitude of the geostrophic wind, and z_0 is the aerodynamic roughness length of the surface. In addition, I will make $\overline{uw}$ and $\overline{vw}$ nondimensional by dividing by u_*^2, where u_* is the friction velocity, a scale I will say much more about later.

Following Tennekes and Lumley (1972, p. 168 ff.), I make eq 16 nondimensional

$$\frac{1}{C_g Ro_*}\frac{\partial U_+}{\partial t_+} = -\frac{\partial\left(\overline{uw}/u_*^2\right)}{\partial z_+} + \frac{1}{C_g Ro_*}\left(V_+ - V_{g+}\right) \tag{46a}$$

$$\frac{1}{C_g Ro_*}\frac{\partial V_+}{\partial t_+} = -\frac{\partial\left(\overline{vw}/u_*^2\right)}{\partial z_+} - \frac{1}{C_g Ro_*}\left(U_+ - V_{g+}\right). \tag{46b}$$

Here

$$C_g \equiv \frac{u_*}{G} \tag{47}$$

is the geostrophic drag coefficient, which, as I will show later, is typically 0.03. And

$$Ro_* \equiv \frac{u_*}{f\,z_0} \tag{48}$$

called the friction Rossby number (Tennekes and Lumley 1972, p. 170), is typically of order 10^6 over sea ice.

If our scaling is accurate in eq 46, the terms containing the nondimensional variables should all be of order one. When the first and last terms in each of these two equations, however, are divided by $C_g Ro_*$, terms of order 10^{-4} result. Consequently, in the ASL, all that remains of eq 46 are

$$\frac{\partial\left(\overline{uw}/u_*^2\right)}{\partial z_+} \cong 0 \tag{49a}$$

$$\frac{\partial\left(\overline{vw}/u_*^2\right)}{\partial z_+} \cong 0. \tag{49b}$$

Thus, $\overline{uw}$ and $\overline{vw}$ are basically constant with height in the ASL. We usually align the x axis with the mean wind so $\overline{vw} = 0$ and then define

$$u_*^2 = -\overline{uw}. \tag{50}$$

Thus, u_* is a fundamental velocity scale in the surface layer because it is constant with height.

We can apply the same scaling procedure to eq 38. Here, in addition to eq 44, however, we also need

$$\Theta_+ = \Theta / t_* \tag{51}$$

where t_* is a temperature scale that I will explain shortly. In eq 38, I make $\overline{w\theta}$ nondimensional with $u_* t_*$. The nondimensional form of eq 38 is thus

$$\frac{1}{Ro_+}\frac{\partial \Theta}{\partial t_+} + \frac{\partial\left(\overline{w\theta}/u_* t_*\right)}{\partial z_+} = \frac{1}{PrR_*}\frac{\partial^2 \Theta_+}{\partial z_+^2} \tag{52}$$

where Pr ($\equiv \nu/D$) is the Prandtl number and

$$R_* \equiv \frac{u_* z_0}{\nu} \tag{53}$$

is the roughness Reynolds number.

Again, as with eq 46, $\partial\Theta_+ / \partial t_+$ should be of order one if our scaling is accurate. But in eq 52, $\partial\Theta_+ / \partial t_+$ is divided by 10^6. In the atmosphere, Pr is about 0.7; and over sea ice R_* is rarely smaller than 10, except in very light winds (Andreas and Claffey 1995). Thus, the third term in eq 52 is also small. Consequently, again the turbulence term is all that remains of eq 52 in the ASL

$$\frac{\partial\left(\overline{w\theta}/u_* t_*\right)}{\partial z_+} \cong 0. \tag{54}$$

As a result, $\overline{w\theta}$, the kinematic sensible heat flux, is basically constant with height in the ASL. We define its value as

$$u_* t_* \equiv -\overline{w\theta}. \tag{55}$$

Thus, because it is independent of height, t_* is the fundamental surface-layer temperature scale.

The mean humidity equation, eq 41, yields to the same scaling arguments that the mean temperature equation did. We thus see that $\overline{wq}$, the kinematic latent heat flux, is also independent of height in the ASL. We define its value as

$$u_* q_* \equiv -\overline{wq} \tag{56}$$

which therefore introduces the fundamental surface-layer humidity scale q_*, another quantity that is constant with height.

Following arguments similar to these, Monin and Obukhov (1954) recognized u_* and t_* as fundamental flux scales in the ASL. In light of eq 33, they also took g/T_v to be an important parameter. Lastly, they knew that the height of the observation, z, was a fundamental length scale in the surface layer. Consequently, they hypothesized that all surface-layer statistics should scale with combinations of these four quantities.

We now know, however, that for scaling properties that depend on air density, rather than t_* alone, we need a scale that also includes q_* (Zilitinkevich 1966, Busch 1973). This is the virtual temperature flux scale, t_{v*}, defined from eq 21b as

$$t_{v*} = t_*\left(1 + 0.61\overline{Q}\right) + 0.61\overline{T}\, q_* \tag{57}$$

where $\overline{Q}$ and $\overline{T}$ must be layer-averaged mean values. Because t_* and q_* are constant with height in the surface layer, t_{v*} is too.

From u_*, t_{v*} and g/T_v, it is possible to define a fundamental length scale L that is also a constant in the ASL

$$\frac{1}{L} \equiv \frac{k g t_{v*}}{T_v u_*^2} = \frac{k g}{\overline{T} u_*^2}\left(t_* + \frac{0.61\overline{T}}{1 + 0.61\overline{Q}} q_*\right) \tag{58}$$

where k (= 0.4) is the von Kármán constant. Many call L the Monin-Obukhov length. I prefer, however, to call it the Obukhov length, since Obukhov defined it in print eight years before the Monin-Obukhov (1954) paper appeared (Businger and Yaglom 1971, Obukhov 1971).

On recognizing the dynamical significance of the surface layer scales u_*, t_*, z and L (we have since added t_{v*} and q_*), Monin and Obukhov (1954) speculated that all surface-layer turbulence statistics should behave similarly when properly expressed in terms of these scales (see also Businger 1973, Wyngaard 1973). In particular, Monin-Obukhov similarity quantifies stability effects in the ASL with the nondimensional parameter $z/L \equiv \zeta$. Shortly, when we see that $\partial U / \partial z \equiv u_* / kz$, it will be evident that ζ is the ratio of the buoyant production to the mechanical production (term III to term II) in the turbulent kinetic energy equation, eq 33. Thus, roughly when $|\zeta| > 1$, buoyancy effects dominate mechanical processes in the surface layer; when $|\zeta| < 1$, mechanical effects dominate. When $\zeta < 0$, the surface is heating and, thus, destabilizing the air in the ASL through the turbulent exchange of sensible and latent heat. This process creates unstable stratification. When $\zeta > 0$, the surface is extracting heat from the surface layer and thereby cooling it from below. This results in a stably stratified surface layer.

As a demonstration of the power of Monin-Obukhov Similarity Theory (MOST), let me consider the variances of vertical velocity, $\overline{w^2} \equiv \sigma_w^2$, and temperature, $\overline{\theta^2} \equiv \sigma_t^2$. Theory predicts that when these statistics are properly scaled, they can be functions only of ζ. That is

$$\frac{\sigma_w}{u_*} = f(z/L) \tag{59}$$

$$\frac{\sigma_t}{t_*} = g(z/L) \tag{60}$$

since u_* is our primary velocity scale in the ASL and t_* is our primary temperature scale.

While MOST predicts that $f(\zeta)$ and $g(\zeta)$ should exist, it does not predict their functional forms. Ultimately, these must be evaluated experimentally. MOST does, however, provide some guidance as to the asymptotic behavior of $f(\zeta)$ and $g(\zeta)$. Let me elaborate.

In the so-called free-convection limit, the buoyancy production term in eq 33 swamps the mechanical production term; thus, u_* loses its significance as the fundamental velocity scale. From the remaining fundamental parameters, $\overline{wt_v}$ (or t_{v*}), g/T_v and z, however, it is possible to define a new velocity scale appropriate for the free-convection limit (e.g., Hess 1992)

$$u_f \equiv \left(\frac{z\, g\, \overline{wt_v}}{T_v} \right)^{1/3} . \tag{61}$$

As in eq 55, we can, in turn, define a new temperature scale for the free-convection limit

$$t_f \equiv \frac{\overline{wt}}{u_f} = \left(\frac{T_v \overline{wt}^3}{z\, g\, \overline{wt_v}} \right)^{1/3} . \tag{62}$$

If these are the proper scales in the free-convection limit, making σ_w and σ_t nondimensional with them should yield universal functions. But now, without u_*, we have used all the scales available to us. In other words, without u_*, L cannot be defined; therefore, σ_w/u_f and σ_t/t_f can depend on no other variables. The only conclusion is that they are constants in the free-convection limit

$$\frac{\sigma_f}{u_f} = \text{constant} \tag{63}$$

$$\frac{\sigma_t}{t_f} = \text{constant}. \tag{64}$$

Since u_* must lose its dynamical significance gradually as ζ decreases, a matching region must exist where both eq 59 and 63 and where both eq 60 and 64 are approximately true. Using the definitions eq 58, 61 and 62 thus implies that asymptotically in the free-convection limit

$$\frac{\sigma_w}{u_*} \propto (-\zeta)^{1/3} \tag{65}$$

and

$$\frac{\sigma_t}{|t_*|} \propto (-\zeta)^{1/3}. \tag{66}$$

Again, although MOST was the basis for our deriving these asymptotic expressions, it tells us nothing about the values of the implied proportionality constants. These must be found experimentally.

The opposite extreme from free convection is very stable stratification—in which the vertical density gradient is actually steep enough to suppress vertical exchange. Thus, the eddies reaching a sensor placed at height z are compacted in their vertical dimension and may never have been in contact with the surface. In other words, contrary to near-neutral or unstable conditions, in very stable conditions, z is no longer a meaningful scale; a turbulence sensor placed at height z can make no measurement that tells it where the surface is. Thus, z drops out of our list of surface-layer scales.

Without z, we cannot form the stability parameter z/L. Therefore, the nondimensional standard deviations in vertical velocity and temperature must be independent of stability in very stable conditions

$$\frac{\sigma_w}{u_*} = \text{constant} \tag{67}$$

$$\frac{\sigma_t}{t_*} = \text{constant}. \tag{68}$$

As usual, MOST does not tell us what these constants should be—only that they should exist.

Figure 1 demonstrates the veracity of MOST. Figure 1a shows σ_w/u_* as a function of stability from measurements I made with three-axis and vertical sonic anemometers at the Sevilleta Long-Term Ecological Refuge near Socorro, New Mexico, in August 1991. Figure 1b shows $\sigma_t/|t_*|$ and σ_q/q_*, where σ_q is the standard deviation in specific humidity, measured during the same experiment. Some of the σ_t values came from the temperature fluctuations measured by the three-axis sonic anemometer–thermometer; some came from a 76-μm chromel-constantan thermocouple. The humidity data came from a krypton hygrometer.

In Figure 1a, σ_w/u_* goes as $(-\zeta)^{1/3}$ for $\zeta < -0.4$, as eq 65 predicts. For $\zeta > 0$, σ_w/u_* is almost independent of ζ, as eq 67 suggests.

The data in Figure 1b are more scattered than those in Figure 1a because t_* and q_* also reflect the uncer-

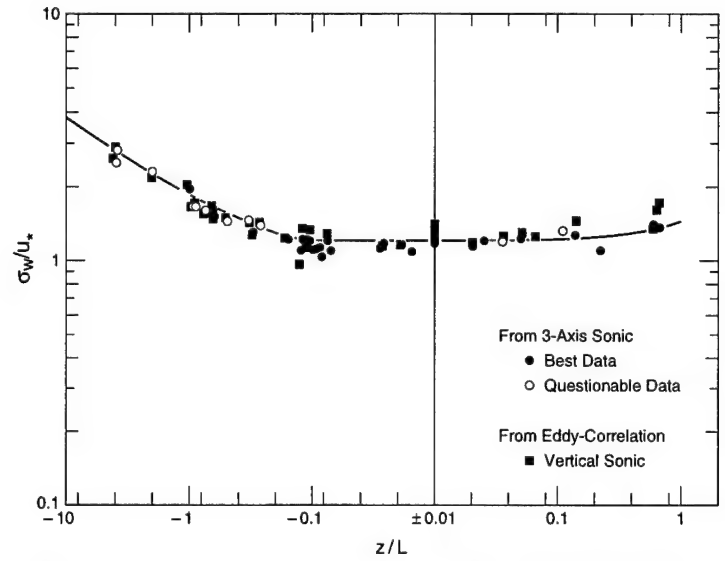

a. Standard deviation of vertical velocity, σ_w. *The line is* $\sigma_w/u_* = 1.20(0.70 - 3.0\zeta)^{1/3}$ *for* $-4 < \zeta \le -0.1$, 1.20 for $-0.1 \le \zeta \le 0$, *and* $1.20(1 + 0.2\zeta)$ *for* $0 \le \zeta < 1$.

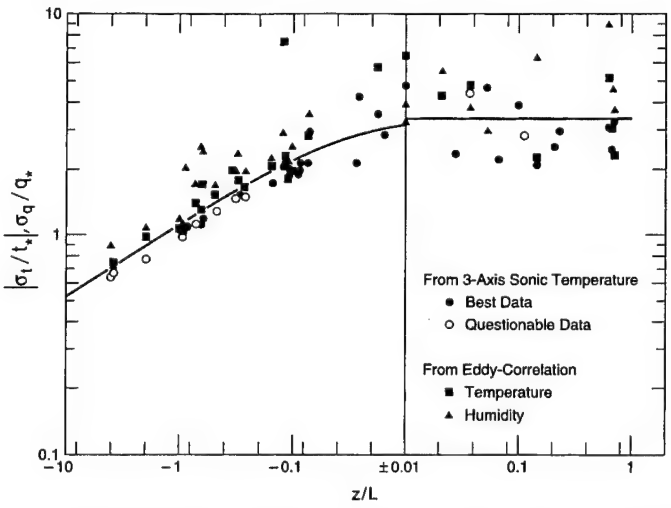

b. *Nondimensional standard deviations of the scalars temperature* (σ_t) *and humidity* (σ_q). *The line is* $\sigma_s/|s_*| = 3.4(1 - 28.4\zeta)^{-1/3}$ *for* $-4 < \zeta \le 0$, *and* 3.4 *for* $0 \le \zeta < 1$.

Figure 1. Demonstration of Monin-Obukhov similarity theory using data collected over a semi-arid grassland in New Mexico in August 1991. One anemometer was a three-axis sonic anemometer–thermometer; the other was a single-axis sonic that was part of an eddy-correlation system manufactured by Campbell Scientific. The three-axis sonic yielded u_* *for nondimensionalizing both sets of* σ_w *measurements. Questionable data were collected in a directionally variable wind.*

tainty in the u_* measurement (see eq 55 and 56). Nevertheless, both the temperature and the humidity data do seem to collapse to a single functional form and, thus, to confirm the predictions of MOST. In particular, for $\zeta < -0.1$, $\sigma_t/|t_*|$ and σ_q/q_* go as $(-\zeta)^{-1/3}$, as eq 66 predicts. And for $\zeta > 0$, the nondimensional standard deviations seem to be independent of ζ.

There have been many other confirmations of Monin-Obukhov similarity theory in the last 30 years (see Haugen [1973] and Panofsky and Dutton [1984] for reviews), and it is now the foundation for our understanding of processes in the atmospheric boundary layer.

SURFACE-LAYER PROFILES

Neutral stratification

Long before the advent of Monin-Obukhov similarity theory, turbulence researchers used scaling arguments to model the wind speed profile in neutral stratification. As I explained, u_* is the fundamental velocity scale in the ASL, and z is a fundamental length scale. In neutral stratification (i.e., when L is infinite or $\overline{wt_v}$ is zero), these are the only scales available to us. Consequently, the vertical gradient in wind speed must obey

$$\frac{dU}{dz} = \frac{u_*}{k\,z} \tag{69}$$

where k, the von Kármán constant, assures the equality.

The no-slip boundary condition means that $U(z)$ is zero at the surface. Hence, we can integrate eq 69 easily to obtain

$$U(z) = \frac{u_*}{z} \ln z + b \tag{70}$$

where b is an integration constant. Because of the logarithm on the right side of eq 70, we cannot write $U(z = 0) = 0$. Rather, we define a new length scale, the roughness length z_0, where $U(z = z_0) = 0$. Thus

$$b = -\frac{u_*}{k} \ln z_0. \tag{71}$$

Consequently

$$U(z) = \frac{u_*}{k} \ln(z / z_0) \tag{72}$$

the familiar semi-logarithmic form of the wind speed profile in neutral stratification.

Figure 2 is a schematic interpretation of eq 72. If we measure U at several heights and plot these data in a coordinate system that is logarithmic in z, the data should lie on a straight line. The slope of this line is u_* / k; it intersects the $U = 0$ axis at $\ln z_0$.

Equation 72, however, is not just a theoretical construct. Semi-logarithmic wind speed profiles are fairly common in nature. Figure 3 shows 10 of the 197 such profiles that Andreas and Claffey (1995) observed over sea ice in the western Weddell Sea.

If $\overline{wt_v}$ is small enough that conditions are still near neutral though t_* (i.e., the sensible heat flux) is nonzero, the potential temperature profile obeys the same scaling as in eq 69. Because t_* is the appropriate temperature scale

$$\frac{d\Theta}{dz} = \frac{t_*}{k\,z}. \tag{73}$$

There is no reason to assume a priori that the same multiplicative coefficient k^{-1} should appear in both eq 69 and 73. In fact, the Kansas results (Businger et al. 1971) showed not only that $k = 0.35$—rather than the more common value of 0.40—but also that there should be an additional multiplicative constant of value 0.74

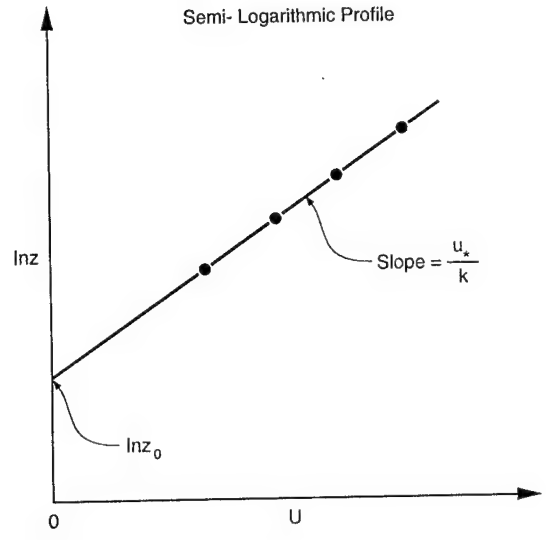

Figure 2. Schematic representation of the semi-logarithmic wind speed profile.

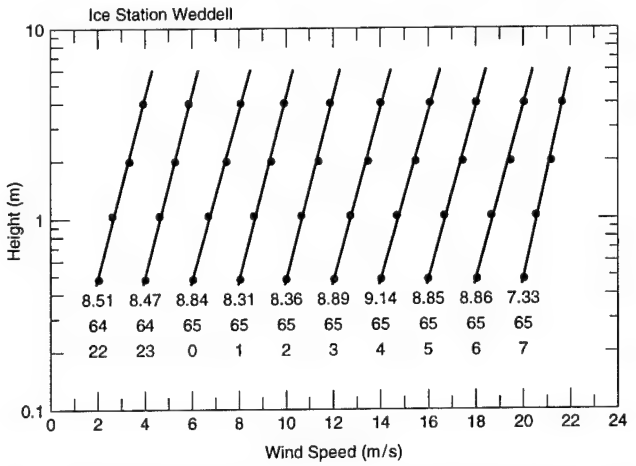

Figure 3. Hourly averaged, semi-logarithmic wind speed profiles observed on Ice Station Weddell (Andreas and Claffey 1995). The lowest level of the left-most profile is assigned a value of 2 m/s; subsequent lowest levels are offset by 2 m/s. Thus, these profiles reflect relative rather than absolute values. The lines are least-squares fits according to eq 72. Under each profile, the upper number is the extrapolated value of the wind speed (in m/s) at 10 m; the middle number is the Julian day in 1992; the lower number is GMT.

on the right side of eq 73. Wieringa (1980), however, reexamined the Kansas data, concluded that $k = 0.41$, nearly the traditional value of 0.40, and found no need for an additional multiplicative constant in eq 73. Högström's (1988) review suggested $k = 0.40 \pm 0.01$ and, again, that eq 69 and 73 represent correct scaling in neutral stratification. Henceforth, I eschew the popular Kansas results and take the more traditional but observationally defensible position that $k = 0.40$ and that the von Kármán constant is the only factor necessary in both eq 69 and 73.

As we did with eq 69, we can integrate eq 73 from the surface to height z. The result is

$$\Theta(z) = T_s + \frac{t_*}{k} \ln z + c \tag{74}$$

where T_s is the surface temperature, and c is a constant of integration. As in eq 71, we find c by requiring Θ to be T_s at the surface; thus

$$\Theta(z) = T_s + \frac{t_*}{k} \ln(z / z_T) \tag{75}$$

where z_T is a new length scale, the roughness length for temperature.

Exactly the same arguments that we used to predict the potential temperature gradient also apply to specific humidity. Thus, in near-neutral stratification

$$\frac{dQ}{dz} = \frac{q_*}{k z}. \tag{76}$$

Integrating this yields

$$Q(z) = Q_s + \frac{q_*}{k} \ln(z / z_Q) \tag{77}$$

where Q_s is the surface value of the specific humidity, and z_Q is yet another length scale, the roughness length for humidity. z_0, z_T and z_Q are not necessarily equal, as I will explain later.

Including stratification effects

Because atmospheric stratification is rarely near neutral, it often affects the shape of surface-layer profiles. Thus, eq 69, 73 and 76 are not strictly accurate in diabatic conditions. We can extend these, however, on the basis of Monin-Obukhov similarity theory. These diabatic profile corrections, in fact, are at the core of Monin and Obukhov's (1954) work. They simply tried to retain the basic form of eq 69, 73 and 76 by multiplying these by functions that depend only on z/L

$$\frac{dU}{dz} = \frac{u_*}{k z} \phi_m(\zeta) \tag{78a}$$

$$\frac{d\Theta}{dz} = \frac{t_*}{k z} \phi_h(\zeta) \tag{78b}$$

$$\frac{dQ}{dz} = \frac{q_*}{k z} \phi_h(\zeta). \tag{78c}$$

As in our earlier discussion, these ϕ functions—though presumably universal—are empirical: They must be found experimentally. Notice, I use the same ϕ function in both the temperature and humidity equations because there is no good theoretical reason why these should be different (Hill 1989). A definitive experiment that verifies this assumption, however, has not been done, though several experiments support it (e.g., Dyer 1974, Dyer and Bradley 1982).

For unstable conditions, ϕ_m and ϕ_h are fairly well known (e.g., Paulson 1970)

$$\phi_m(\zeta) = (1 - 16\zeta)^{-1/4} \tag{79a}$$

$$\phi_h(\zeta) = (1 - 16\zeta)^{-1/2}. \tag{79b}$$

These are commonly called the Businger-Dyer relations because Joost Businger (1966) and Arch Dyer derived them independently in the mid-1960s (Businger 1988). Though the constant multiplying ζ in eq 79 may vary somewhat among the various experimental evaluations of ϕ_m and ϕ_h (e.g., Dyer and Hicks 1970, Businger et al. 1971, Wieringa 1980, Dyer and Bradley 1982, Högström 1988), the same basic functional form comes through.

Figure 4 shows eq 79 as functions of stability. Notice in the figure and in eq 79, $\phi_m = \phi_h = 1$ at $\zeta = 0$ (i.e., for neutral stratification) as eq 69, 73, and 76 require. Figure 4 also shows that as $-\zeta$ gets larger—as conditions become more unstable—both ϕ_m and ϕ_h

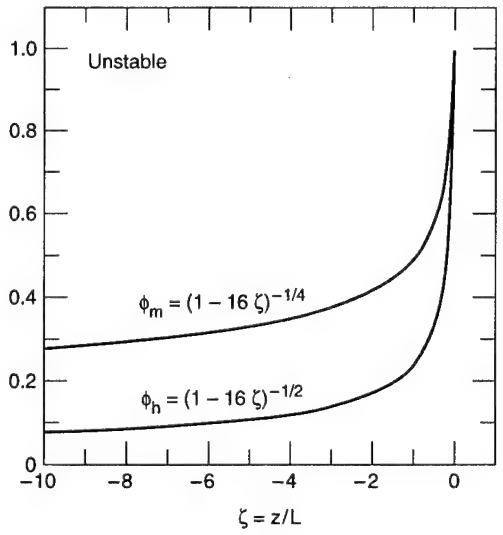

Figure 4. Nondimensional wind speed and scalar gradients, ϕ_m and ϕ_h, as functions of stability for unstable conditions.

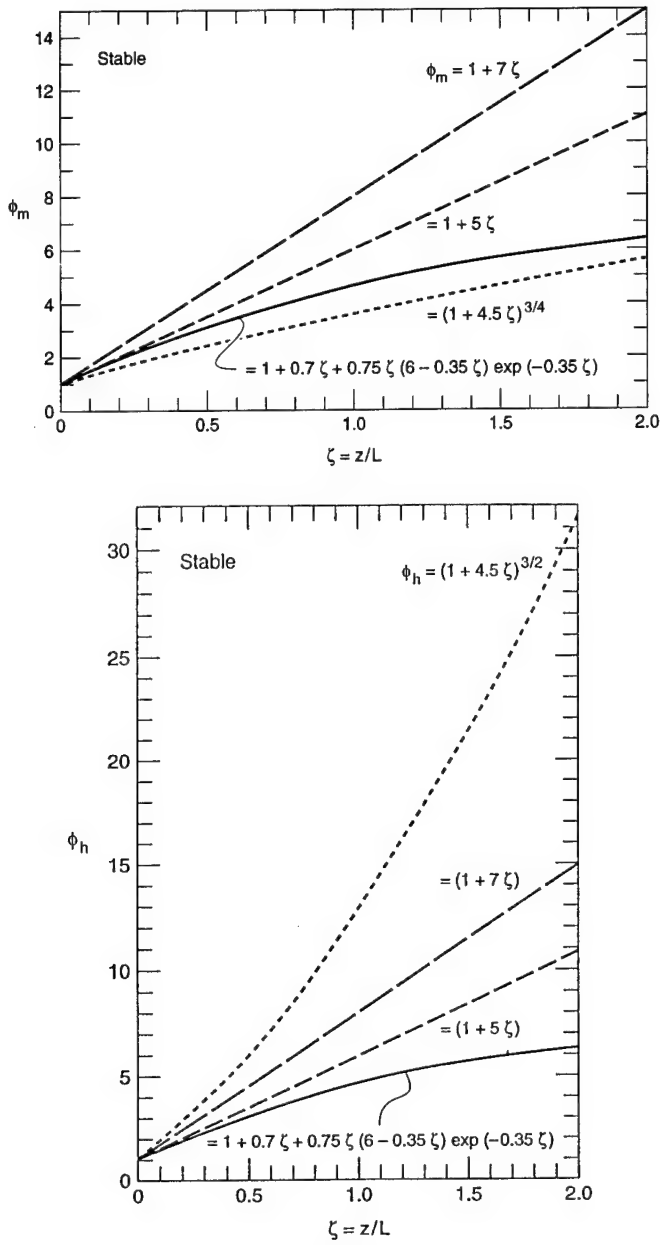

Figure 5. Various suggestions for the functional form of the nondimensional wind speed (ϕ_m) and scalar (ϕ_h) gradients for stable conditions.

decrease monotonically. This means, according to eq 78, that the vertical gradients of wind speed, temperature and humidity get weaker as the instability increases. The vertical exchange that the increasing buoyancy fosters homogenizes the profiles.

In contrast to the situation for unstable stratification, for an ASL that is stably stratified there are a host of suggestions as to the forms of ϕ_m and ϕ_h. Figure 5 shows some of these functions.

Often the wind speed and scalar profiles are assumed to be log-linear in stable conditions (Webb 1970). That is, the profiles are basically semi-logarithmic as in eq 72, 75 and 77, but each has an additional additive term that depends on ζ. ϕ_m and ϕ_h would, thus, have the form

$$\phi_m(\zeta) = \phi_h(\zeta) = 1 + \gamma_s\zeta. \tag{80}$$

The constant γ_s is generally reported to be in the range from 5 (Webb 1970, Dyer 1974, Large and Pond 1981) to 7 (Wieringa 1980, Large and Pond 1982, Högström 1988).

From wind speed and temperature profiles at the South

Pole, Lettau (1979) deduced the nondimensional gradient functions

$$\phi_m(\zeta) = (1 + 4.5\zeta)^{3/4} \tag{81}$$

and

$$\phi_h(\zeta) = \phi_m(\zeta)^2 = (1 + 4.5\zeta)^{3/2} \tag{82}$$

which are also depicted in Figure 5. Lettau's ϕ_h function predicts a very steep scalar gradient with increasing ζ that has not been confirmed by independent observations.

Although Lettau (1979) developed his functions especially to treat very stable conditions, the log-linear form (eq 80) is also often applied in very stable conditions, though it has been tested only for $0 \le \zeta < 1$ (e.g., Dyer 1974, Hicks 1976, Yaglom 1977). As an alternative to the log-linear form for $0 \le \zeta \le 10$, Holtslag and de Bruin (1988) and Beljaars and Holtslag (1991) proposed the function

$$\begin{aligned}\phi_m(\zeta) &= \phi_h(\zeta) \\ &= 1 + 0.7\zeta + 0.75\zeta(6 - 0.35\zeta)\exp(-0.35\zeta).\end{aligned} \tag{83}$$

I will refer to this as the Dutch formulation.

In Figure 5, we see that there is little difference among the four functions suggested for ϕ_m and ϕ_h when $0 \le \zeta \le 0.5$. Thus, because the log-linear form is much simpler mathematically than Lettau's (1979) or the Dutch formulation, it might be preferable for weakly stable conditions. Some other considerations, however, might help us decide which of the four formulations is best in more stable conditions.

The gradient Richardson number is

$$Ri = \frac{g}{T_v}\frac{\partial\Theta / dz}{(\partial U / dz)^2}. \tag{84}$$

From eq 78 and the definition of ζ (eq 58) we can write this as

$$Ri = \frac{g}{T_v}\frac{(t_* / kz)\phi_h(\zeta)}{(u_* / kz)^2 \phi_m^2(\zeta)} = \frac{\zeta\phi_h(\zeta)}{\phi_m^2(\zeta)}. \tag{85}$$

In stable conditions, turbulence ceases when the Richardson number exceeds a critical value, Ri_{cr}. Thus, we should expect accurate profile functions to yield this critical value through eq 85; that is

$$\lim_{\zeta\to\infty} Ri = Ri_{cr}. \tag{86}$$

Traditionally, Ri_{cr} is assumed to be 0.20–0.25 (Busch 1973, Businger 1973). But Mahrt (1981) and Heinemann and Rose (1990) have reported that a larger value is sometimes indicated. Woods (1969) may have explained this range of values by demonstrating that there is a hysteresis in Ri_{cr}. He concluded that a turbulent flow becomes laminar when Ri exceeds 1, but a laminar flow does not become turbulent until Ri falls below 0.25 (see also Plate 1971, p. 76). In his observations at South Pole, however, Lettau (1979) frequently found turbulence to exist even when Ri exceeded unity; he thus concluded that, in stable conditions, there was no critical Richardson number. Monin and Yaglom (1971, p. 440 f.) also argued that there seems to be no critical Richardson number in stable conditions. In light of this controversy, I show in Table 1 what the four formulations for ϕ_m and ϕ_h depicted in Figure 5 predict as the behavior of Ri in very stable conditions.

Table 1. Predicted behavior of the Deacon and Richardson numbers in very stable conditions according to the four gradient formulation shown in Figures 4 and 5.

	limit $\zeta \to \infty$		
ϕ_m, ϕ_h	D_m	D_h	Ri
$1 + 5\zeta$	0	0	$1/5 = 0.20$
$1 + 7\zeta$	0	0	$1/7 = 0.14$
$\phi_m = (1 + 4.5\zeta)^{3/4}$ $\phi_h = (1 + 4.5\zeta)^{3/2}$	$1/4$	$-1/2$	ζ
$1 + 0.7\,\zeta + 0.75\zeta(6 - 0.35\zeta)\exp(-0.35\zeta)$	0	0	1.4

Lettau (1979; see also Viswanadham [1979, 1982]) described two other parameters that characterize surface-layer profiles, the Deacon numbers for wind speed and potential temperature, D_m and D_h, respectively. These quantify profile curvature. For wind speed

$$D_m \equiv \frac{-z(d^2U / dz^2)}{dU / dz}. \tag{87}$$

With eq 78a, it is easy to show that

$$D_m(\zeta) = 1 - \frac{\zeta}{\phi_m(\zeta)}\frac{d\phi_m(\zeta)}{d\zeta}. \tag{88}$$

Similarly, for potential temperature

$$D_h \equiv \frac{-z(d^2\Theta / dz^2)}{d\Theta / dz} \tag{89}$$

which, with eq 78b, becomes

$$D_h(\zeta) = 1 - \frac{\zeta}{\phi_h(\zeta)}\frac{d\phi_h(\zeta)}{d\zeta}. \tag{90}$$

Table 1 also shows the Deacon numbers that the four ϕ_m and ϕ_h formulations in Figure 5 predict in very stable conditions.

Table 1 yields contradictory suggestions as to which of the ϕ_m and ϕ_h formulations is best in stable conditions. The Webb (1970) and Wieringa (1980) functions predict that Ri_{cr} is 0.20 and 0.14, respectively—roughly the traditional range for Ri_{cr} (Lumley and Panofsky 1964, p. 117). The Dutch formulation predicts $Ri_{cr} = 1.4$, a value in line with more recent appraisals. The critical Richardson number based on Lettau's (1979) formulation is unbounded, a result that Monin and Yaglom (1971, p. 441) defended theoretically and that Lettau believed was possible in light of his South Pole observations.

In very stable conditions, turbulence is suppressed; the vertical exchange of heat and momentum must thus be by molecular processes alone. In such conditions, the vertical profiles of wind speed and temperature depend linearly on height, and their vertical gradients are, thus, constants with height; D_m and D_h would then be zero. Viswanadham's (1982) analysis also suggested that zero is the limiting value, at least for D_m, in very stable conditions. (He did not consider D_h.) In Table 1, three of the formulations predict that zero is the limit for the Deacon numbers in strong stability. But, again from his measurements at South Pole, Lettau (1979) found that $D_m = {}^1/_4$ and $D_h = -{}^1/_2$ in very stable conditions and, therefore, tuned his ϕ_m and ϕ_h functions to produce these limits.

In stable stratification, wave phenomena can supplant forced convection and molecular diffusion as the dominant mechanisms for transferring heat and momentum. These processes are necessarily intermittent. The stratification builds and builds, until a wave breaks and introduces new turbulence that episodically homogenizes the wind speed and temperature profiles. The overriding stratification eventually damps this turbulence until the cycle repeats. Thus, it seems that all the limiting Deacon and Richardson numbers listed in Table 1 may be appropriate at times. The very steep temperature gradient that Lettau (1979) reported would be consistent with a relatively quiet, strongly stratified surface layer. But the weaker gradient of the Dutch formulation seems plausible, too, in a surface layer frequently mixed by breaking gravity waves. Thus, the stable atmospheric surface layer is still rife with interesting questions about turbulence processes.

BULK TRANSFER COEFFICIENTS FOR HEAT AND MOMENTUM OVER SEA ICE

Mathematical background

For estimating turbulent surface fluxes from field data, in computer models, and for some analytical studies, it is often convenient to know the so-called bulk transfer coefficients. These relate a turbulent flux to more readily available quantities.

Here, I will discuss the bulk transfer coefficients for momentum (usually called the drag coefficient) and for sensible and latent heat. These are defined, respectively, as

$$\tau = -\rho\,\overline{uw} = \rho u_*^2 = C_{Dr}\,\rho U_r^2 \tag{91}$$

$$H_s = \rho c_p\,\overline{wt} = -\rho c_p u_* t_* = C_{Hr}\,\rho c_p U_r\,(T_s - \Theta_r) \tag{92}$$

$$H_L = \rho L_v\,\overline{wq} = -\rho L_v u_* q_* = C_{Er}\,\rho L_v U_r (Q_s - Q_r). \tag{93}$$

In these c_p = specific heat of air at constant pressure
L_v = latent heat of vaporization or sublimation
T_s, Q_s = surface values
U_r, Θ_r, Q_r = values at some reference height, usually 10 m
C_{Dr}, C_{Hr} and C_{Er} = bulk transfer coefficients. Since these are height dependent, I explicitly include a height subscript in their symbols.

In the last section, I introduced the gradient functions $\phi_m(\zeta)$ and $\phi_h(\zeta)$ in eq 78. These let us quantify U_r, $T_s - \Theta_r$ and $Q_s - Q_r$ in eq 91–93 and thereby provide a mathematical framework for handling the bulk transfer coefficients. Take wind speed as an example. From eq 78a

$$\frac{dU}{dz} = \frac{u_*}{kz}\phi_m(z/L). \tag{94}$$

Panofsky (1963) and Paulson (1970) showed how to integrate this. The trick is to write

$$\frac{dU}{dz} = \frac{u_*}{kz}\left[1 - 1 + \phi_m(\zeta)\right] \tag{95}$$

then the integration becomes

$$\int_{U(z_0)}^{U(z)} dU' = \frac{u_*}{k}\left[\int_{z_0}^{z}\frac{dz'}{z} - \int_0^{\zeta}\frac{1-\phi_m(\zeta')}{\zeta'}\,d\zeta'\right]. \tag{96}$$

Hence, because $U(z_0) = 0$

$$U(z) = \frac{u_*}{k}\left[\ln(z/z_0) - \psi_m(\zeta)\right]. \tag{97}$$

Thus, the trick in eq 95 leads again to a semi-logarithmic profile with an additive stability correction. That stability correction in eq 97, ψ_m, is defined as

$$\psi_m(\zeta) = \int_0^{\zeta} \frac{1-\phi_m(\zeta')}{\zeta'} d\zeta'. \tag{98}$$

We can follow exactly the same procedure with the potential temperature and specific humidity gradients in eq 78b and 78c to obtain the profiles of these variables

$$\Theta(z) = T_s + \frac{t_*}{k}\left[\ln(z/z_T) - \psi_h(\zeta)\right] \tag{99}$$

$$Q(z) = Q_s + \frac{q_*}{k}\left[\ln(z/z_Q) - \psi_h(\zeta)\right] \tag{100}$$

where

$$\psi_h(\zeta) = \int_0^{\zeta} \frac{1-\phi_h(\zeta')}{\zeta'} d\zeta'. \tag{101}$$

To see the ψ_m and ψ_h functions that result from integrating the ϕ_m and ϕ_h functions that I described in the last sections, see Paulson (1970), Lettau (1979), Holtslag and de Bruin (1988), Arya (1988, p. 166 f.), or Launiainen and Vihma (1990).

Figures 6 and 7 show sample wind speed and potential temperature profiles computed from eq 97 and eq 99. Note the curvature of the unstable wind speed and temperature profiles. The vertical exchange characteristic of unstable stratification tends to homogenize the profiles; both wind speed and temperature bend more towards the vertical with increasing height. In stable conditions, on the other hand, the stratification suppresses vertical exchange. Consequently, steeper gradients are possible.

From eq 91–93, 97, 99 and 100, we see that the bulk transfer coefficients are clearly stability dependent (e.g., Andreas and Murphy 1986)

$$C_{Dr} = \frac{k^2}{[\ln(r/z_0) - \psi_m(r/L)]^2} \tag{102}$$

$$C_{Hr} = \frac{k^2}{[\ln(r/z_0) - \psi_m(r/L)]\,[\ln(r/z_T) - \psi_h(r/L)]} \tag{103}$$

$$C_{Er} = \frac{k^2}{[\ln(r/z_0) - \psi_m(r/L)]\,[\ln(r/z_Q) - \psi_h(r/L)]} \tag{104}$$

At neutral stability ($r/L = 0$) both ψ_m and ψ_h are zero by definition. Such conditions define the neutral-stability bulk transfer coefficients. From eq 102–104, these are

$$C_{DNr} = \frac{k^2}{[\ln(r/z_0)]^2} \tag{105}$$

$$C_{HNr} = \frac{k^2}{[\ln(r/z_0)][\ln(r/z_T)]} = \frac{k\,C_{DNr}^{1/2}}{\ln(r/z_T)} = \frac{C_{DNr}}{1 - k^{-1}\,C_{DNr}^{1/2}\ln(z_T/z_0)} \tag{106}$$

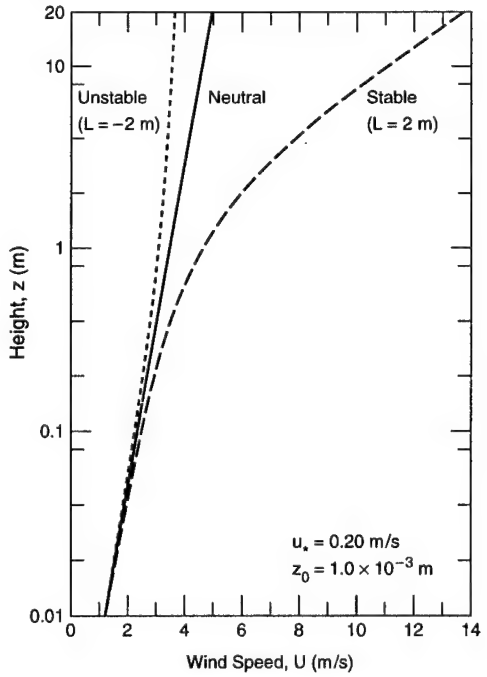

Figure 6. Sample wind speed profiles. Conditions are as labeled. The ψ_m in eq 97 is based on the Businger-Dyer form (eq 79 and Figure 4) for the unstable case and on the Dutch formulation (eq 83 and Figure 5) for the stable case.

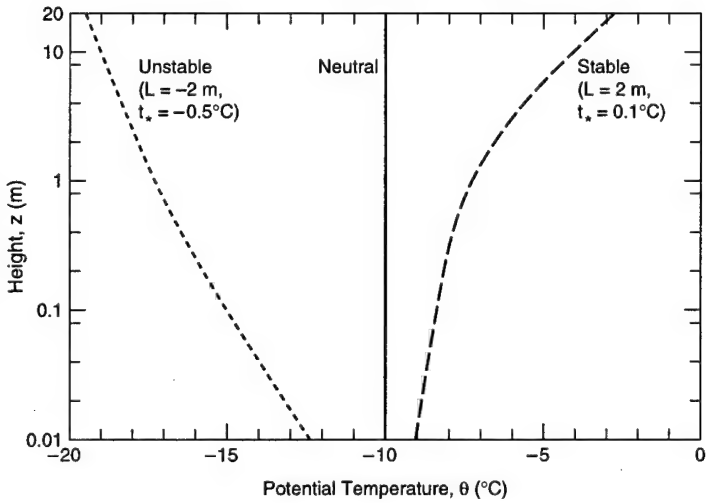

Figure 7. Sample potential temperature profiles. Conditions are as labeled. The ψ_m in eq 97 is based on the Businger-Dyer form (eq 79 and Figure 4) for the unstable case and on the Dutch formulation (eq 83 and Figure 5) for the stable case.

$$C_{ENr} = \frac{k^2}{[\ln(r/z_0)][\ln(r/z_Q)]} = \frac{k\,C_{DNr}^{1/2}}{\ln(r/z_Q)} = \frac{C_{DNr}}{1 - k^{-1}\,C_{DNr}^{1/2}\ln(z_Q/z_0)}. \quad (107)$$

Thus, knowing z_0, z_T and z_Q is equivalent to knowing the neutral-stability bulk transfer coefficients for any reference height r.

We also see from eq 106 and 107 that equality of z_0, z_T and z_Q implies that $C_{DNr} = C_{HNr} = C_{ENr}$. Although some measurements have suggested that $C_{HNr} = C_{ENr}$, none have confirmed that C_{DNr} is, in general, equal to either of these, as I will explain shortly. Thus, equality between z_0 and z_T or z_Q is not true either.

From eq 102–104, it is clear that if we know the neutral-stability transfer coefficients or z_0 and z_T and z_Q, we know the stability-dependent transfer coefficients needed in eq 91–93 to compute the turbulent fluxes of interest. Deardorff (1968) was one of the first to show plots of the bulk transfer coefficients as functions of stability. More recently, Smith (1988) presented updated plots using modern expressions for the necessary similarity functions. In a nutshell, for constant wind speed, C_D, C_H and C_E all increase as conditions become more unstable; and, again for a constant wind speed, all decrease as stability increases. These results follow intuitively from our discussion of how vertical exchange is enhanced in unstable conditions and suppressed in stable conditions.

Since we can obtain the bulk transfer coefficients at any height and for any stratification from the roughness lengths or from the neutral-stability coefficients, we can confine the rest of our discussion to the values of these neutral-stability coefficients. I will also settle on the standard reference height of 10 m and, henceforth, confine my discussion to the neutral-stability transfer coefficients at 10 m, C_{DN10}, C_{HN10} and C_{EN10}. For completeness, the following equations show how to compute C_{Dr}, C_{Hr} and C_{Er} from these neutral-stability values (Andreas and Murphy 1986)

$$C_{Dr} = \frac{C_{DN10}}{\left\{1 + k^{-1}\,C_{DN10}^{1/2}\,[\ln(r/10) - \psi_m(r/L)]\right\}^2} \quad (108)$$

$$C_{Hr} = \frac{C_{DN10}(C_{Dr}/C_{DN10})^{1/2}}{1 + k^{-1}\,C_{HN10}\,C_{DN10}^{-1/2}[\ln(r/10) - \psi_h(r/L)]} \quad (109)$$

$$C_{Er} = \frac{C_{EN10}(C_{Dr}/C_{DN10})^{1/2}}{1 + k^{-1}\,C_{EN10}\,C_{DN10}^{-1/2}[\ln(r/10) - \psi_h(r/L)]} \quad (110)$$

where r must be expressed in meters.

Drag coefficient

Overland (1985) reviewed 45 evaluations of the drag coefficient over sea ice published through 1984. Since then, Anderson (1987), Fairall and Markson (1987), Guest and Davidson (1987, 1991), Martinson and Wamser (1990), Wamser and Martinson (1993), Andreas et al. (1993b), and Andreas and Claffey (1995) have added to this information pool.

But I still feel that one of the most important works on this subject is that by Banke et al. (1980). They showed that C_{DN10} is related to a measurable surface roughness parameter ξ through (Fig. 8)

$$10^3\,C_{DN10} = 1.10 + 0.072\xi \quad (111)$$

where ξ must be in centimeters. Here, ξ obtains from an integration under the snow-surface roughness spectrum, Φ_s

$$\xi^2 = \int_{\kappa_0}^{\infty} \Phi_s(\kappa)\,d\kappa \quad (112)$$

where κ is the wavenumber and $\kappa_0 = 0.5$ rad/m, which corresponds to a maximum wavelength of about 13 m.

In turn, the snow-surface roughness spectrum, $\Phi_s(\kappa)$, is the spectral density (Andreas et al. 1993b) obtained from a Fourier analysis of a snow-surface elevation profile. Figure 9 shows such a snow-surface elevation profile and the actual ice-surface elevation profile measured on Ice Station Weddell (ISW) in 1992 (Anonymous 1992, ISW Group 1993). Figure 10 shows the resulting (nondimensional) snow-surface (Φ_s) and ice-surface (Φ_i) roughness spectra implied by these profiles (see Andreas et al. [1993b] for computational guidelines). According to eq 112, ξ is obtained from the Φ_s line in Figure 10 by integrating from $\kappa = 0.5$ rad/m to infinity. That upper integration limit, however, is not actually infinity but rather the Nyquist wavenumber $2\pi/2\Delta$, where Δ is the sampling interval. Since Banke et al. (1980) used a sampling interval of 1 m, for their ξ values the upper integration limit was π rad/m. Because the sampling interval for the ISW profiles was 0.5 m, however, the Nyquist wavenumber for these is 2π rad/m (Fig. 10).

Figure 8 and eq 111 suggest that form drag is important in fostering momentum exchange. As the surface gets measurably rougher, there are more vertical surfaces for the wind to push against; C_{DN10} consequently increases. Measurements in the 1980s in the marginal ice zone—arguably the roughest oceanic surface—corroborated this hypothesis that as the surface gets visibly rougher the drag coefficient increases (Andreas et al. 1984; Brown 1986, 1990; Anderson 1987; Guest and Davidson 1987, 1991).

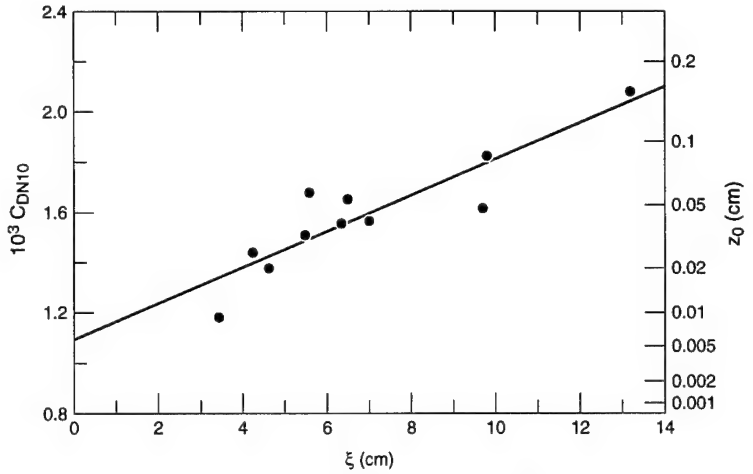

Figure 8. The 10-m, neutral-stability drag coefficient (C_{DN10}) over Arctic sea ice is related to a parameter that characterizes surface roughness (ξ) (after Banke et al. 1980).

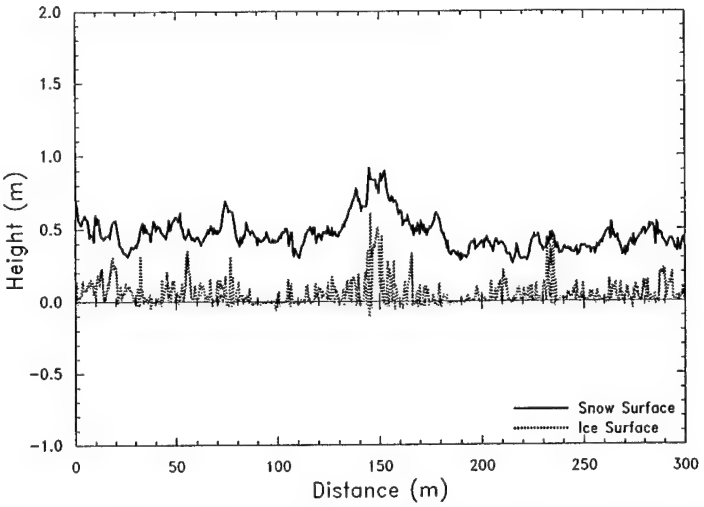

Figure 9. A 300-m-long snow-surface and ice-surface elevation profile measured on Ice Station Weddell.

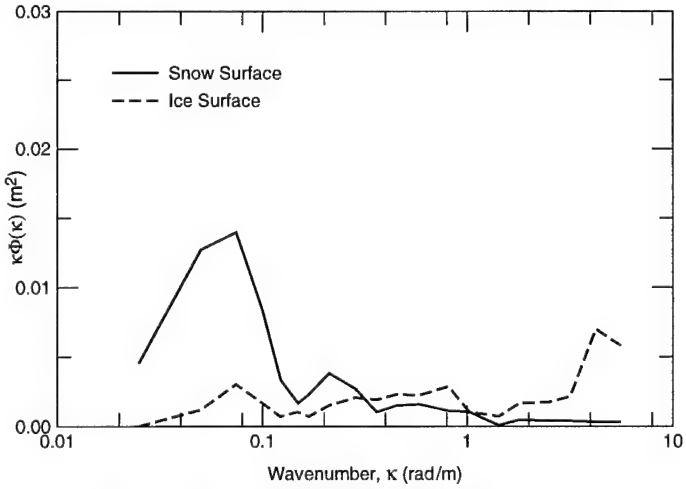

Figure 10. Snow-surface and ice-surface roughness spectra computed for the profiles in Figure 9. For the snow-surface spectrum, ξ = 3.7 cm.

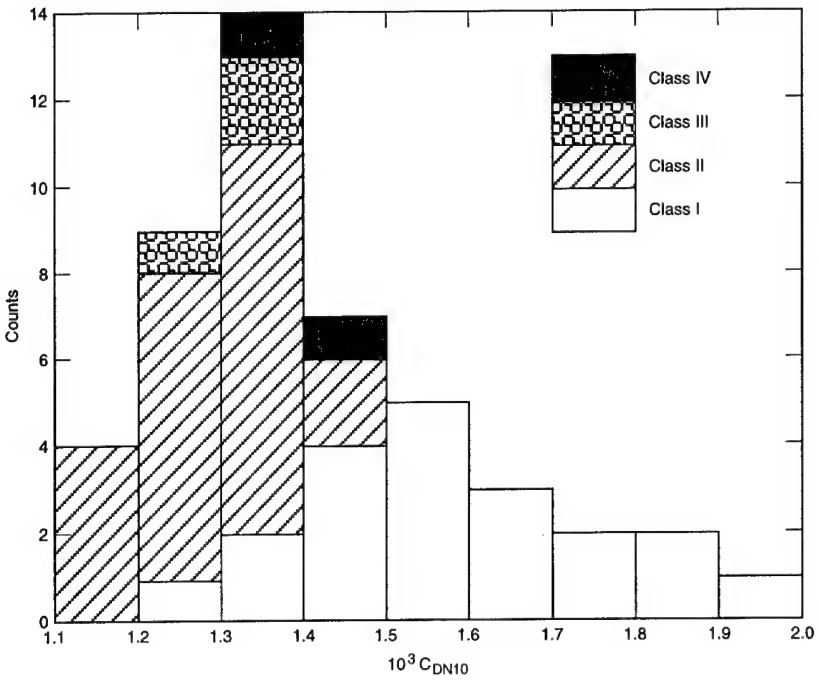

Figure 11. Neutral-stability, 10-m air–ice drag coefficients computed from eq 111 using snow-surface elevation profiles collected during the Winter Weddell Gyre Study (Andreas et al. 1993b).

The power of eq 111 is its implicit suggestion that it may be possible to determine the drag coefficient remotely from instruments sensitive to surface roughness. In this light, eq 111 warranted further investigation. The Winter Weddell Gyre Study (WWGS; Augstein et al. 1991) on the *Polarstern* gave us an opportunity to try this inverse use of eq 111. During a 1989 transect of the Weddell Sea, WWGS scientists collected 47 snow-surface profiles like that in Figure 9, except most were only about 100 m long. We computed Φ_s from these, then ξ from eq 112, and finally C_{DN10} from eq 111 (Andreas et al. 1993b). Figure 11 shows a histogram of the resulting values.

Lange and Eichen (1991) had developed a classification scheme for sea ice in the Weddell Sea. They identified four ice classes, as follows:

Class I: deformed first-year ice
Class II: undeformed first-year ice
Class III: undeformed second-year (multiyear) ice
Class IV: deformed second-year (multiyear) ice

In Figure 11, I distinguish the drag coefficients computed for each ice class. Because WWGS scientists had little opportunity to sample second-year floes, the statistics on classes III and IV in the figure are uncertain. But for classes I and II, where the sample size is larger, Figure 11 corroborates our earlier speculation: When the ice is identifiably rougher (i.e., deformed), the drag coefficient is generally larger.

Much of the appeal of eq 111 is the unification it provides; it confirms our intuition about the importance of roughness on drag with hard data. Unfortunately, no one has found independent confirmation of eq 111 (e.g., Shirasawa 1981). The actual form of eq 111 may be a moot point, however. Our recent observations on Ice Station Weddell in the western Weddell Sea imply that eq 111 oversimplifies air–ice coupling.

Figure 12 is a time series of ISW C_{DN10} values that Andreas and Claffey (1995) deduced from four-level wind speed profiles, including those in Figure 3. Though

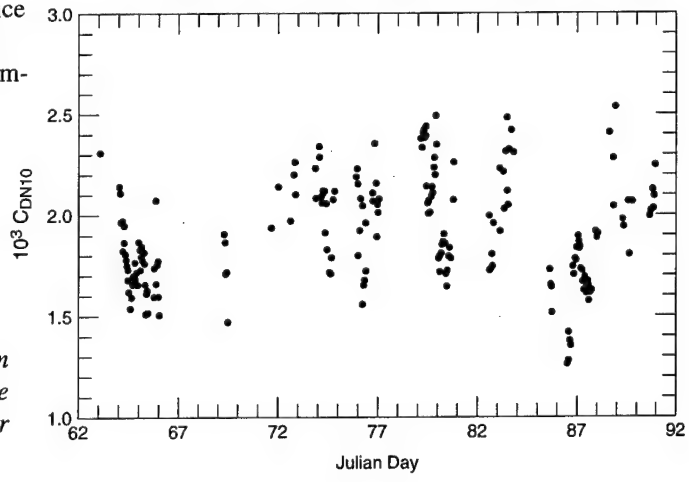

Figure 12. Time series of the neutral-stability, 10-m drag coefficient measured on a fixed mast on Ice Station Weddell (see Andreas and Claffey [1995] or Andreas [1995a]).

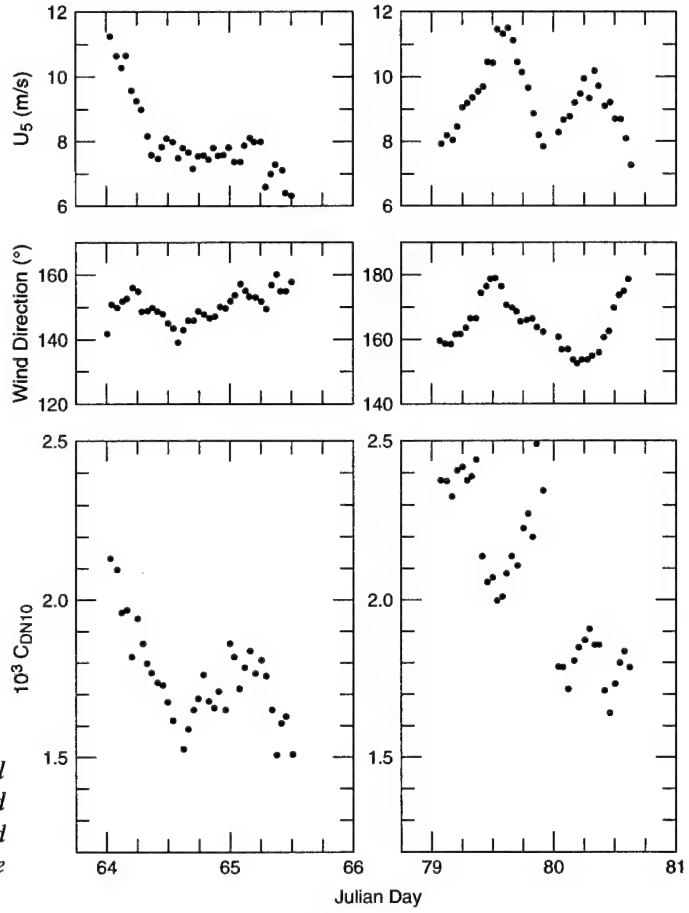

Figure 13. Two long events on Ice Station Weddell that were characterized by a relatively constant wind direction (hourly average). U_5 *is the hourly averaged wind speed at a height of 5 m; the* C_{DN10} *values came from Figure 12.*

these data came from a single mast that did not move with respect to the surrounding ice for the duration of the experiment, the C_{DN10} values range from 1.27×10^{-3} to 2.54×10^{-3}. And these values are not randomly scattered but rather behave coherently with time. Figure 13 shows two long storm events extracted from Figure 12. In each case, C_{DN10} decreased as the wind persisted from a fairly constant direction and blew with speeds of about 8 m/s or higher.

On ISW we observed that snow generally began drifting when the wind at 5 m reached 6 m/s. When the wind reached 8–10 m/s, blowing and drifting snow were virtually guaranteed. Figure 14 summarizes these observations.

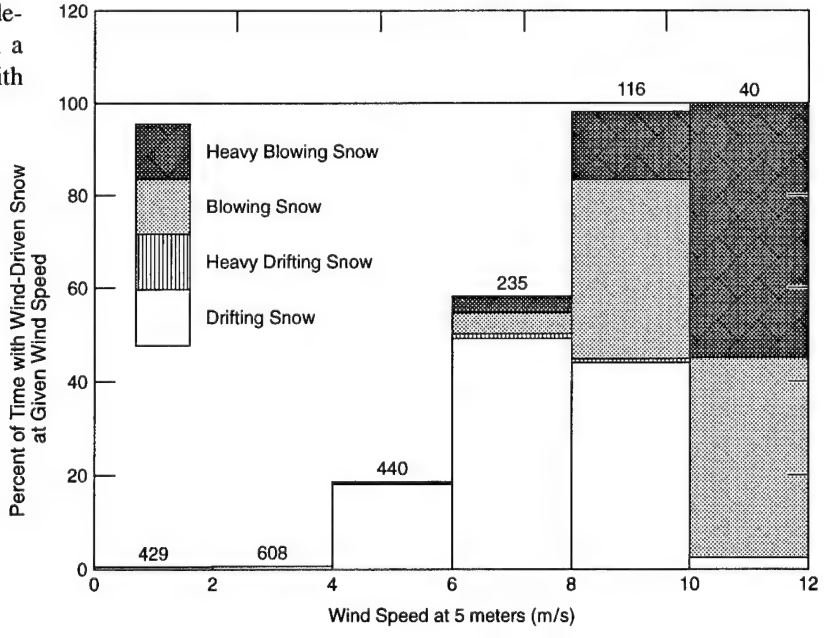

Figure 14. Ice Station Weddell observations showing the percentage of the time with wind-driven snow for a given 5-m wind speed. The terminology follows National Weather Service (1991) guidelines. Above each histogram bar is the number of hourly averaged wind speeds within the indicated range.

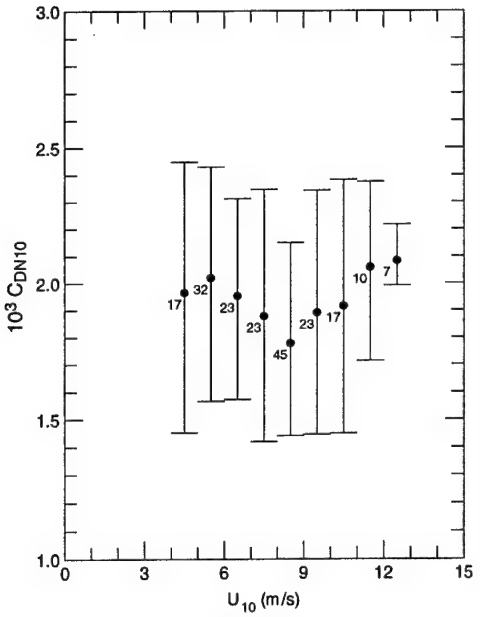

Figure 15. C_{DN10} *values in Figure 12, averaged over 1-m/s bins of the 10-m wind speed; the filled circle denotes this average. Next to each circle is the number of* C_{DN10} *values in each bin. The vertical bar indicates the 90% confidence interval for the population within each bin, assuming a beta distribution with lower limit* 1.2×10^{-3} *and upper limit* 2.60×10^{-3} *(Harr 1977, p. 495 f.).*

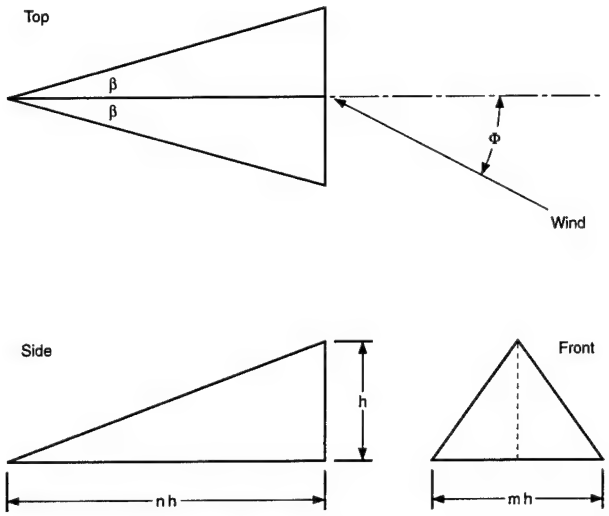

Figure 16. Geometry of the sastrugi-like roughness elements envisioned to dictate the drag coefficient over snow-covered sea ice. If the wind has been blowing above 6–8 m/s for 10–12 hours, the sastrugi will be aligned with the mean wind direction; Φ *will then be* 0°.

We thus inferred that, for most of the hourly values depicted in Figure 13, wind-driven snow was present (Andreas and Claffey 1995). As a result, the decrease in the C_{DN10} values during the two events suggests that snowdrifts perpendicular to the wind were eroding, and this snow was depositing in drifts that tended to streamline the surface in the mean wind direction. This streamlining lowered the aerodynamic roughness and therefore the drag coefficient.

Visual inspection of Figure 13 may suggest that the behavior of C_{DN10} is simply a wind speed effect: Lower C_{DN10} values seem to be associated with lower wind speeds. But looking at the entire ISW set of drag coefficients (Fig. 15) does not corroborate this speculation. C_{DN10} does not have any obvious dependence on the wind speed for speeds between 4 and 14 m/s. Likewise, Shirasawa (1981) found no wind speed dependence in drag coefficients measured over snow-covered lake ice for winds up to 11 m/s, and Inoue (1989) also found no wind speed dependence at Mizuho Station on the Antarctic continent for winds up to about 15 m/s.

To investigate further this hypothesis that streamlining of the surface by wind-driven snow has a major effect on the air–ice drag coefficient, I (Andreas 1995a, 1995b) developed a physically based form drag model following Raupach's (1992) guidelines. Figure 16 depicts the rudimentary sastrugi-like roughness elements that I treat with the model. Although we made no formal observations of sastrugi or surface texture on ISW, we often saw that high wind sculpted the snow surface into linear drifts that looked like Figure 16. Figure 9 supports these casual observations; it shows that the snow collected around protrusions in the sea ice surface but that the resulting drifts were generally small. Hence, I assume that the typical sastrugi height, h in Figure 16, was roughly 10–15 cm on ISW.

Figure 17 shows model predictions of how C_{DN10} depends on the wind's orientation with respect to the long axis of the sastrugi (Φ in Fig. 16). In the figure, γ is the fractional surface coverage of the roughness elements depicted in Figure 16. Notice, because of the geometry of the modeled sastrugi, the maximum possible value of γ is 0.50.

Figure 17 reproduces some of the observations that I have been describing. When the wind is well aligned (within ±15°) with the sastrugi, C_{DN10} has a minimum. As the wind turns to blow more perpendicularly to the sastrugi (without being high enough to erode them), C_{DN10} increases. For $h = 15$ cm and $\gamma = 0.15$, the model predicts C_{DN10} values in line with what we observed on ISW. The model yields $C_{DN10} = 1.43 \times 10^{-3}$ when the wind is within ±12° of head-on to the sastrugi, while on

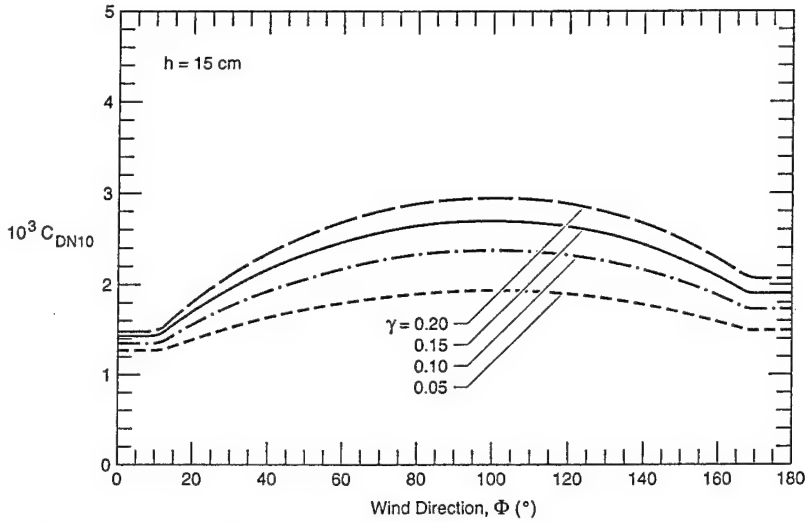

Figure 17. Model calculations of the neutral-stability, 10-m drag coefficient, C_{DN10}, as a function of the wind orientation, Φ, with respect to the dominant axis of the sastrugi depicted in Figure 16 (from Andreas 1995a,b). Here, the sastrugi height, h, is 15 cm; and γ is the fraction of the surface that the sastrugi cover. Also, m = 4 and n = 10 (see Fig. 16).

ISW the minimum C_{DN10} value was about 1.5×10^{-3}. When the wind is roughly at a right angle to the sastrugi, the model predicts a maximum in C_{DN10} of 2.70×10^{-3}, while our observed maximum was 2.54×10^{-3}.

Our ISW observations and this modeling have, thus, shown some deficiencies in eq 111. Because drifting snow makes a sea ice surface anisotropic, eq 111 can be true only if ξ is obtained from a snow-surface profile aligned with the mean wind. But our observations and modeling also reiterate one of the conclusions implicit in eq 111: Small roughness elements (heights of order 10–15 cm) with fairly short wavelengths (order of meters) dominate the local form drag over snow-covered surfaces. Jackson and Carroll (1978) had reached the same conclusion. Because the horizontal scales involved are much smaller than either Arctic or Antarctic ridge spacings (Lytle and Ackley 1991), pressure ridges seem to be less important in local processes. Nevertheless, pressure ridges may still be important in setting the large-scale roughness and drag coefficient over sea ice (Arya 1973, 1975).

Scalar bulk transfer coefficients

The Reynolds analogy (Schlichting 1968, p. 268 f. and 662 f.; Hinze 1975, p. 746) is the hypothesis that momentum and scalars, such as temperature or humidity, are transferred similarly. An immediate conclusion of the Reynolds analogy is that $C_{DN10} = C_{HN10} = C_{EN10}$. In discussing eq 105–107, however, I noted that, in geophysical flows at least, C_{DN10} has never been proven to equal C_{HN10} or C_{EN10}. The reason is that, over natural surfaces, momentum and scalars are transferred by different processes.

Figure 18 is a depiction of the microscale of a natural surface such as snow. The surface has millimeter-size roughness elements that sometimes are embedded in the viscous sublayer and sometimes protrude above the viscous sublayer. The roughness Reynolds number, eq 53, parameterizes the aerodynamic character of a surface. When $R_* \leq 0.135$, the surface is aerodynamically smooth; when $R_* \geq 2.5$, the surface is aerodynamically rough; when $0.135 < R_* < 2.5$, the surface is in transition (Businger 1973).

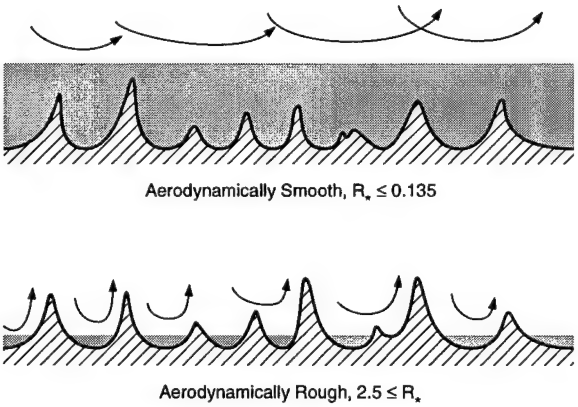

Figure 18. Schematic depiction of the microscale roughness of an aerodynamically smooth and an aerodynamically rough surface. The shading shows the viscous sublayer, where momentum transfer to the surface must be by molecular processes.

Physically, what these distinctions mean are that when the surface is aerodynamically smooth, the roughness elements are embedded in the viscous sublayer; as a result, momentum is transferred to the surface strictly by molecular processes. When the surface is aerodynamically rough, the roughness elements protrude through the viscous sublayer; turbulent eddies can therefore transfer momentum through pressure forces on the roughness elements as well as through molecular processes. In eq 33, term IVb reflects this explicit dependence of the TKE budget on transfers resulting from the covariance of velocity and pressure fluctuations. We find no similar pressure transport terms in either the temperature variance budget, eq 39, or the humidity variance budget, eq 42. Scalars cannot be transported by pressure forces; scalar transfer at a surface is always molecular. Consequently, over aerodynamically rough surfaces, at least, the Reynolds analogy is inherently inappropriate (cf., Joffre 1982).

Measurements have not yielded conclusive results on the behavior of the scalar transfer coefficients over snow-covered surfaces. Hicks and Martin (1972) and Thorpe et al. (1973) measured both C_{HN10} and C_{EN10} over lake ice and sea ice, respectively. Joffre (1982) measured C_{HN10} over snow-covered sea ice. Kondo and Yamazawa (1986) measured C_{HN1} (1-m value) and Barry and Munn (1967) measured $C_{EN0.3}$ (30-cm value) over snow-covered ground. The inferred C_{HN10} and C_{EN10} values are quite scattered because, over snow, the potential temperature and humidity gradients necessary to compute the transfer coefficients (see eq 92 and 93) are generally small and, thus, difficult to measure precisely. The C_{HN10} values from the measurements are typically about 1×10^{-3}, but C_{EN10} measurements do not suggest a consensus value. Andreas (1987) reviewed some of these observations.

In the absence of definitive experimental work, I devised a model to predict C_{HN10} and C_{EN10} (Andreas 1987). My work built on Brutsaert's (1975a, b) surface-renewal model. Its main result is to predict the scalar roughness, z_s, as a function of z_0 and R_*

$$\ln(z_s / z_0) = b_0 + b_1 \ln R_* + b_2 (\ln R_*)^2 \qquad (113)$$

where Table 2 gives the polynomial coefficients when z_s is z_T or z_Q. Figure 19 shows this equation.

We see from eq 106 and 107 that knowing z_T/z_0 and z_Q/z_0 is essential for predicting C_{HNr} and C_{ENr}. But we also see from these equations that both scalar transfer coefficients also depend on C_{DNr}. Hence, to use eq 113 in eq 106 and 107 to predict C_{HN10} and C_{EN10}, I used eq 111 to model C_{DN10} (Andreas 1987). As a result, both scalar transfer coefficients depend on wind speed (because z_s/z_0 depends on R_*) and ξ. Figure 20 shows model predictions of C_{HN10} and C_{EN10}.

Table 2. Values of the coefficients in the polynomial (eq 113) that predicts z_T/z_0 and z_Q/z_0.

	$R_* \le 0.135$	$0.135 < R_* < 2.5$	$2.5 \le R_* \le 1000$
Temperature (z_T/z_0)			
b_0	1.250	0.149	0.317
b_1	—	–0.550	–0.565
b_2	—	—	–0.183
Water vapor (z_Q/z_0)			
b_0	1.610	0.351	0.396
b_1	—	–0.628	–0.512
b_2	—	—	–0.180

Figure 20 shows not only C_{HN10} and C_{EN10} but also C_{DN10} computed from eq 111, which is independent of wind speed. Only at very low wind speeds, when the flow is aerodynamically smooth or in transition, are C_{HN10} and C_{EN10} near C_{DN10}—the Reynolds analogy. For higher winds, C_{HN10} and C_{EN10} are clearly less than C_{DN10}. Figure 19 shows the same behavior; z_T and z_Q can be orders of magnitude less than z_0 as the flow gets more aerodynamically rough.

Munro (1989) verified some of the predictions of this model with data collected over a Canadian glacier. Kondo and Yamazawa's (1986) data collected over snow-covered ground provide another test of the model's prediction of C_{HN10} (Fig. 20a). Because Kondo and Yamazawa reported only C_{HN1} and C_{DN1} (both at

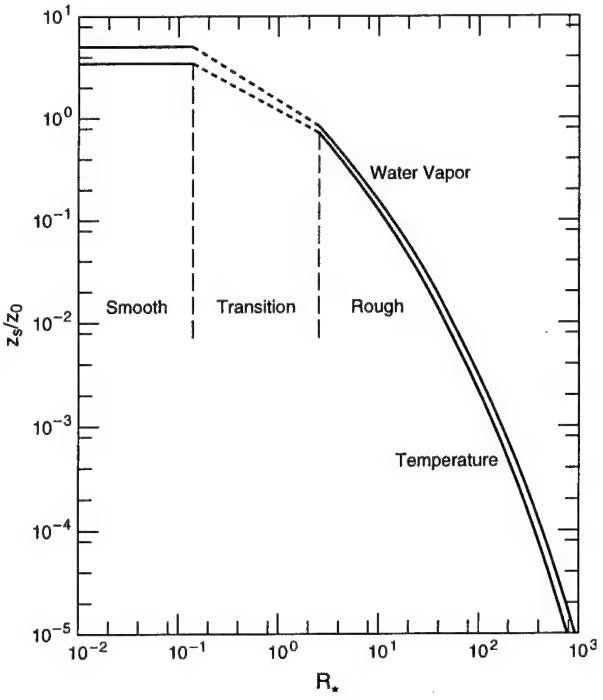

Figure 19. Model predictions of z_T/z_0 and z_Q/z_0 over snow-covered surfaces (from Andreas 1987). The three regions label where the flow is aerodynamically smooth, aerodynamically rough, or in transition.

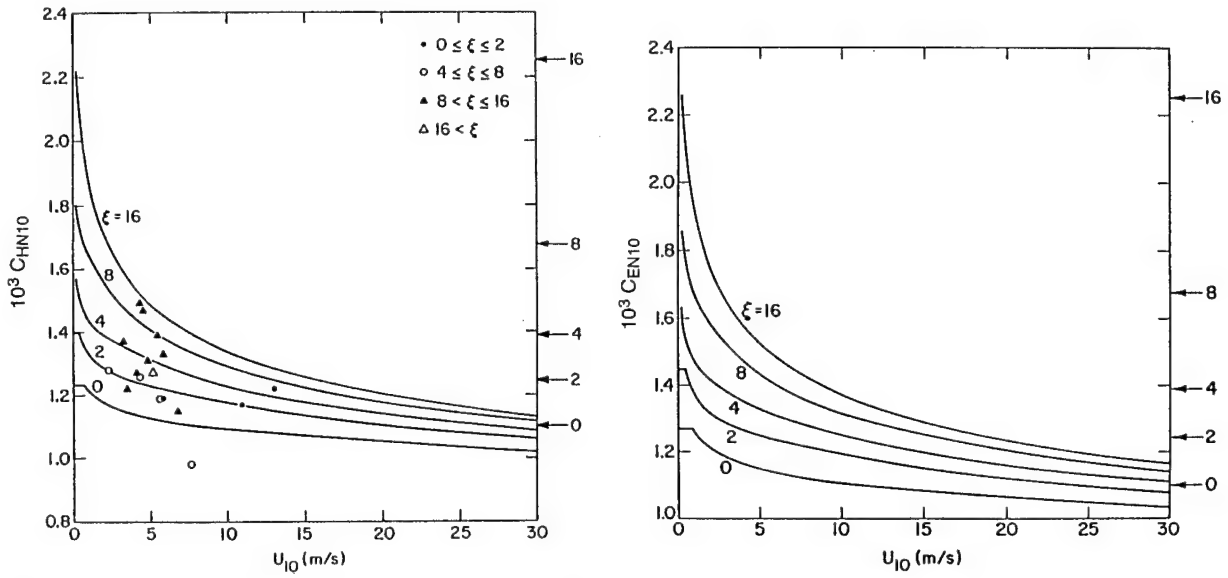

a. C_{HN10}. *The data points are from measurements by Kondo and Yamazawa (1986).*

b. C_{EN10}.

Figure 20. Model predictions (from Andreas 1987) of C_{HN10} *and* C_{EN10} *over snow-covered surfaces as a function of the surface roughness parameter* ξ *(in cm) and the 10-m wind speed,* U_{10}. *The arrows on the right show* C_{DN10} *for the indicated* ξ *value.*

1 m), I had to obtain their raw data* to compute the points plotted in Figure 20a. In addition, because they had not measured ξ, I inferred the ξ values associated with the C_{HN10} values in Figure 20a by using eq 111 to estimate ξ from their measured drag coefficients.

Although there are some discrepancies between the model predictions and the data in Figure 20a, the comparison is quite encouraging. The data support the model prediction that C_{HN10} increases with increasing C_{DN10} at a given wind speed and that C_{HN10} decreases with increasing wind speed. Unfortunately, no high quality measurements are yet available for testing the model's prediction for C_{EN10}, though several have accepted its predictions for both C_{HN10} and C_{EN10} (Morris 1989, Munro 1989, Launiainen and Vihma 1990).

THE EKMAN LAYER

Polar meteorology has, of course, relied on the discoveries of meteorologists working at lower latitudes. But, in turn, meteorologists and oceanographers everywhere owe a debt to a polar scientist, Fridtjof Nansen. During the drift of the *Fram* across the Arctic Ocean in the mid-1890s (Nansen 1897), Nansen noticed that his ship and the sea ice generally drifted to the right of the wind. Ekman (1905) developed a mathematical explanation for these observations and thereby provided meteorology and oceanography with the first rigorous planetary boundary layer model. Though the spiral in the wind vector that Ekman's model predicts is rarely seen, his model is still a basis for current ABL modeling. Hence, I will describe it in some detail here.

Start with eq 16, which are equations for the mean horizontal wind vector. Assuming steady-state simplifies these, but the turbulence terms still make analytic solution difficult. We, thus, need a closure assumption. The Ekman solution is to assume that the turbulent transport can be modeled as a turbulent diffusion process with a constant turbulent diffusivity K. That is, the surface stresses in the x and y directions, τ_x and τ_y, are modeled as

$$\tau_x / \rho = -\overline{uw} = K \frac{\partial U}{\partial z} \tag{114a}$$

$$\tau_y / \rho = -\overline{vw} = K \frac{\partial V}{\partial z}. \tag{114b}$$

With these and the assumption of steady-state, eq 16 yield (e.g., Stull 1988, p. 210 f.; Garratt 1992, p. 42)

$$-f(V - V_g) = K \frac{\partial^2 U}{\partial z^2} \tag{115a}$$

$$f(U - U_g) = K \frac{\partial^2 V}{\partial z^2} \tag{115b}$$

* Personal communication with J. Kondo, Professor of Meteorology, Geophysical Institute, Tohoku University, Sendai, Japan, 1986.

or

$$-f(V-V_g)=K\frac{\partial^2(U-U_g)}{\partial z^2} \tag{116a}$$

$$f(U-U_g)=K\frac{\partial^2(V-V_g)}{\partial z^2} \tag{116b}$$

since U_g and V_g are independent of height.

If we define

$$S\equiv(U-U_g)+i(V-V_g) \tag{117}$$

we can combine eq 116 a and b into one equation in S

$$\frac{if\,S}{K}=\frac{\partial^2 S}{\partial z^2}. \tag{118}$$

The solution of this is easiest if we align the x axis with the geostrophic wind, that is, $V_g = 0$. Then the boundary conditions at $z = 0$ are

$$U(0)=V(0)=0 \tag{119}$$

so

$$S(0)=-U. \tag{120}$$

As z approaches infinity, the boundary conditions are

$$\lim_{z\to\infty} U(z)=U_g \tag{121a}$$

$$\lim_{z\to\infty} V(z)=0 \tag{121b}$$

so

$$\lim_{z\to\infty} S(z)=0. \tag{122}$$

With these boundary conditions, the solution of eq 118 is fairly straightforward. It is (e.g., Businger 1982; Stull 1988, p. 211; Garratt 1992, p. 42)

$$U(z)=U_g[1-\exp(-z/\delta)\cos(z/\delta)] \tag{123a}$$

$$V(z)=sgnf\,U_g\exp(-z/\delta)\sin(z/\delta). \tag{123b}$$

Here, *sgnf* is the sign of the Coriolis parameter: plus in the Northern Hemisphere, minus in the Southern Hemisphere. And δ is a height scale

$$\delta=\left(\frac{2K}{|f|}\right)^2. \tag{124}$$

Let us look at what eq 123 implies about processes at the surface. From eq 114 and 123, we see that

$$\tau_x/\rho=\frac{KU_g}{\delta} \tag{125a}$$

$$\tau_y/\rho=\frac{-KU_g\,sgnf}{\delta}. \tag{125b}$$

That is, the surface stress is to the right of the geostrophic wind in the Northern Hemisphere, as Nansen observed; in the Southern Hemisphere, it is to the left. Since by definition

$$\tau=\left(\tau_x^2+\tau_y^2\right)^{1/2}=\rho u_*^2 \tag{126}$$

we also find from eq 125 another relation between the constants

$$u_*^2=\frac{2^{1/2}KU_g}{\delta}. \tag{127}$$

Using this in eq 124, we see that

$$\delta=\frac{2^{1/2}u_*^2}{|f|U_g}. \tag{128}$$

While solving the Ekman equations in the geostrophic wind frame is easiest, observers at the surface know the direction of the surface stress (remember, in an Ekman layer the surface wind vector is zero) better than they know the direction of the geostrophic wind. Hence, for me at least, it is easier to visualize the Ekman winds in a coordinate system aligned with the surface stress vector than in a coordinate system aligned with the geostrophic wind. The following equations accomplish this transformation of velocity components in the geostrophic wind frame [denoted as (U,V)] to components in the surface stress frame [denoted as (U',V')]:

$$U'(z)=2^{-1/2}[U(z)+sgnf\,V(z)] \tag{129a}$$

$$V'(z)=2^{-1/2}[-sgnf\,U(z)+V(z)]. \tag{129b}$$

Thus, substituting eq 123 into eq 129 yields the Ekman solution in a reference frame aligned with the surface stress

$$U'(z)=2^{-1/2}G \times\{1-\exp(-z/\delta)[\cos(z/\delta)-\sin(z/\delta)]\} \tag{130a}$$

$$V'(z)=-2^{-1/2}G\,sgnf \times\{1-\exp(-z/\delta)[\cos(z/\delta)+\sin(z/\delta)]\} \tag{130b}$$

Here, G is the magnitude of the geostrophic wind; and, in this frame, the y component of the geostrophic wind is no longer zero. Thus

$$G = U_g = \left(U_g'^2 + V_g'^2\right)^{1/2}. \tag{131}$$

Figure 21 shows plots of eq 130 in both the Northern and Southern Hemispheres. The obvious feature in these hodographs is the so-called Ekman spiral. The height of the Ekman layer, h_E, is commonly taken as

$$h_E = \pi\,\delta \tag{132}$$

since $\pi\,\delta$ is the lowest height at which the velocity vector has the same direction as the geostrophic wind (see Fig. 21). From eq 128, we can estimate that h_E is on the order of 300 m.

We see in Figure 21 that the Ekman winds turn with increasing height. In a Cartesian coordinate system with positive angles counterclockwise from the x axis, the turning angle α between the surface stress and the geostrophic wind is given by

$$\tan\alpha = \lim_{z\to\infty} \frac{V'(z)}{U'(z)} = -sgnf \tag{133}$$

or

$$\alpha = -45°\ sgnf. \tag{134}$$

The geostrophic wind makes a 45° angle with the surface stress in an Ekman layer.

That 45° turning angle is easy to remember; remembering the direction of the turning, however, is harder since some of us deal with ABLs in both hemispheres. Thus, I find it helpful to bring some of the sophistication of physics to boundary-layer meteorology through the following right-hand rule.

Figure 22 presents another view of the Ekman solution. Notice, the longitudinal velocity component is dis-

A Right-Hand Rule for the Ekman Layer

1. Point the fingers of the right hand in the direction of the surface stress.
2. Curl the fingers in the direction of *f*. (*f* is up in the Northern Hemisphere; down in the Southern Hemisphere.)
3. The right thumb then points in the direction that the wind will turn with increasing height in an Ekman layer.

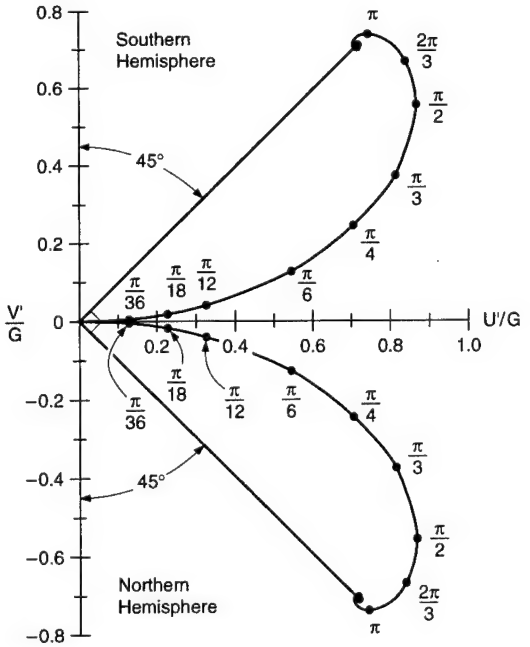

Figure 21. Hodographs of the wind vector in Ekman layers in the Northern and Southern Hemispheres. The dots with numbers nearby mark nondimensional heights, z/δ. The straight line at 45° in each hemisphere shows the geostrophic wind.

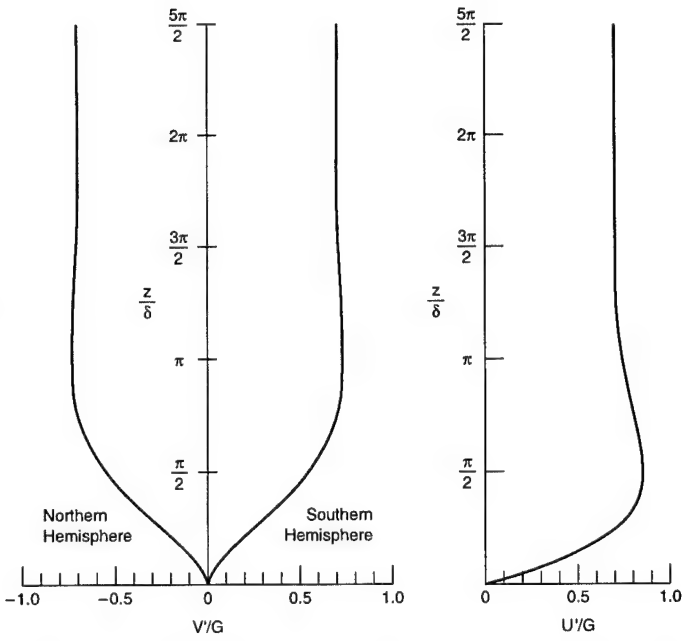

Figure 22. Nondimensional profiles of the longitudinal and transverse velocity components for Ekman layers in the Northern and Southern Hemispheres. The x *(or* U′*) axis is aligned with the surface stress.*

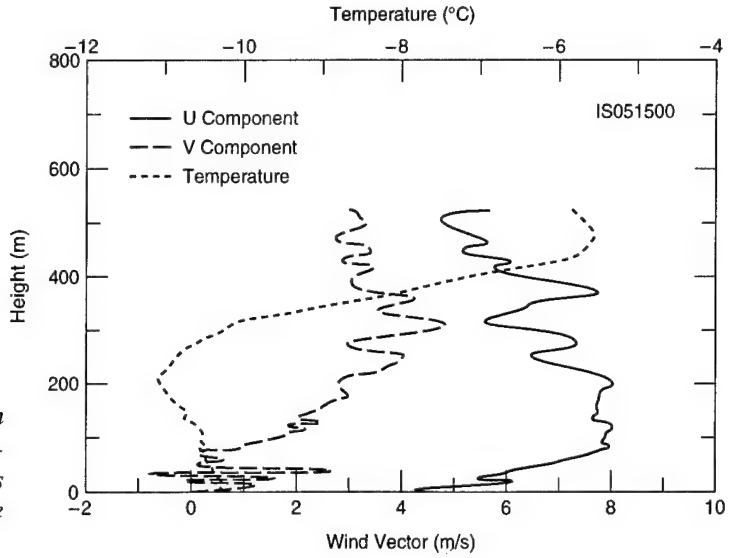

Figure 23. The 00 GMT radiosounding from Ice Station Weddell on 15 May 1992. The coordinate system is such that the surface wind has no transverse component (i.e., the coordinate system is aligned with the surface stress).

tinctly supergeostrophic; it has a bulge near $z/\delta = \pi/2$ where $U' > U'_g$. The transverse velocity component is also a bit supergeostrophic just below $z/\delta = \pi$. Notice, too, for $z > \pi\delta = h_E$, the wind vectors are approximately geostrophic.

The question now becomes: How realistic is the Ekman solution; is the Ekman spiral, for example, ever observed in nature? We made a lot of radiosounding profiles on Ice Station Weddell (Claffey et al. 1994); it would be reasonable to look through these for evidence of an Ekman layer. But remember, the Ekman layer is derived assuming neutral stratification. On ISW, stable stratification was the norm. Figure 23 does, however, show one ISW radiosounding that found a nearly neutral layer 200 m deep. In this layer, the wind clearly turns counterclockwise with height, as Figure 21 suggests it should in the Southern Hemisphere. But since the upper-level wind components have different magnitudes, the turning angle is not the 45° predicted for an Ekman layer; it is actually closer to 30°. Nevertheless, there are enough similarities between Figure 23 and the Ekman model—the turning, the height over which the turning occurs—for us to see that the essence of the model must be correct. For an even better demonstration of the veracity of the Ekman solution, see McPhee and Martinson (1994). They observed a fairly well behaved Ekman spiral in the oceanic boundary layer under the sea ice at ISW.

THERMAL WIND

Many phenomena are present in the atmosphere that void the assumptions on which Ekman based his model. Thus, the paucity of observations of a true atmospheric Ekman layer is not surprising. The thermal wind is one such phenomenon that complicates the analytical description of the ABL.

Remember, eq 15 defined the geostrophic wind components. Suppose, rather than being constant as Ekman assumed, the geostrophic wind varies with height. On using the ideal gas law, eq 5, and taking the z derivative in eq 15, we can show (e.g., Arya and Wyngaard 1975; Sorbjan 1989, p. 177 f.)

$$\frac{\partial U_g}{\partial z} = \frac{-g}{fT}\frac{\partial T}{\partial y}\bigg|_P = \frac{-g}{f}\frac{\partial \ln T}{\partial y}\bigg|_P \tag{135a}$$

$$\frac{\partial V_g}{\partial z} = \frac{g}{fT}\frac{\partial T}{\partial x}\bigg|_P = \frac{g}{f}\frac{\partial \ln T}{\partial x}\bigg|_P \tag{135b}$$

where the subscript P indicates that the derivatives are along surfaces of constant pressure. If these terms are not zero, meteorologists say that there is a thermal wind or geostrophic shear; oceanographers prefer to describe this effect as baroclinicity. The terms are all equivalent (Arya and Wyngaard 1975).

For the terms in eq 135 to be nonzero, we see that a horizontal temperature gradient must exist. In other words, a surface that is not horizontally homogeneous in temperature will induce thermal wind effects. How do these effects manifest?

By integrating eq 135 from the surface to height z, we get the following

$$U_g(z) = U_g(0) - \frac{g}{f}\int_0^z \frac{\partial \ln T}{\partial y}\,dz' \tag{136a}$$

$$V_g(z) = V_g(0) + \frac{g}{f}\int_0^z \frac{\partial \ln T}{\partial x}\,dz' \tag{136b}$$

where, for convenience, I have dropped the subscript P that appeared in eq 135. For illustrative purposes, suppose

$$\frac{\partial \ln T}{\partial y} = m \tag{137a}$$

$$\frac{\partial \ln T}{\partial x} = n \tag{137b}$$

where m and n are constants (e.g., Sorbjan 1989, p. 179). Then eq 136 simply become

$$U_g(z) = U_g(0) - mgz/f \tag{138a}$$

$$V_g(z) = V_g(0) + ngz/f. \tag{138b}$$

That is, in this example, the baroclinicity causes the geostrophic wind components to increase or decrease with height depending on the direction of the gradient in surface temperature.

Again, it is hard for me to remember the direction in which the geostrophic wind will change in response to a surface temperature gradient. I, thus, developed another right-hand rule.

For practice with this rule, suppose you are over sea ice in the Weddell Sea (i.e., in the Southern Hemisphere). There is open water to the east; thus, the positive temperature gradient points east. Suppose the surface geostrophic wind is blowing due north. According to the above rule, V_g must increase with height to the south. That is, $V_g(z)$ will get smaller with height and may even turn negative (i.e., the wind may blow toward the south at some height).

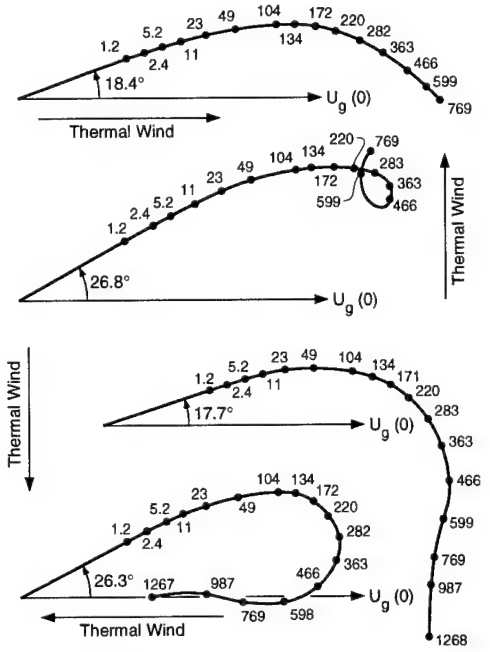

Figure 24. Northern Hemisphere hodographs of Ekman spirals in the presence of a constant thermal wind. The thermal wind effect is modeled as in eq 138; the magnitude of the plotted thermal wind vector is roughly mgz/f (*or* ngz/f) *for z of 800–900 m. The surface-level geostrophic wind is labeled* $U_g(0)$. *The numbers near the dots indicate the height in meters (after Blackadar 1963; see also Brown 1974).*

A Right-Hand Rule for the Thermal Wind

1. Point the fingers of the right hand in the direction of *f*. (*f* is up in the Northern Hemisphere; down in the Southern Hemisphere.)
2. Curl the fingers in the direction of the positive temperature gradient.
3. The right thumb then points in the direction in which the geostrophic wind increases with height.

Sorbjan (1989, p. 179 f.) showed how to incorporate simple thermal wind parameterizations like eq 138 into the Ekman solutions. The result is a distorted Ekman spiral whose shape depends on the relative magnitudes and directions of the surface geostrophic wind and the horizontal temperature gradient. Figure 24 shows some similarly modified Ekman spirals from Blackadar (1963). Clearly, the presence of a thermal wind can hide the Ekman spiral.

ROSSBY NUMBER SIMILARITY

As I have hinted, the Ekman solution has shortcomings. In particular, it predicts a low-speed layer at the surface that is fairly thick (see Fig. 22). In reality, the wind speed increases rapidly above the surface; at a height of only 1 m, it is already an appreciable fraction of the geostrophic wind speed (e.g., see Fig. 6). Conversely, the surface-layer profiles I described in earlier sections are not accurate for heights above, roughly, $^1/_{10}$ the height of the ABL. Blackadar and Tennekes (1968), however, demonstrated that, by matching surface-layer and Ekman-layer solutions in a region where they overlap, it is possible to mathematically describe the entire ABL with an extended Ekman solution that also treats stability effects.

We can write the surface-layer solutions eq 97, 99 and 100 as

$$\frac{U(z)}{u_*} = \frac{1}{k}\left[\ln(z/z_0) - \psi_m(\zeta)\right] \tag{139a}$$

$$\frac{V(z)}{u_*} = 0 \tag{139b}$$

$$\frac{\Theta(z) - T_s}{t_*} = \frac{1}{k}\left[\ln(z/z_T) - \psi_h(\zeta)\right] \tag{140}$$

$$\frac{Q(z) - Q_s}{q_*} = \frac{1}{k}\left[\ln(z/z_Q) - \psi_h(\zeta)\right]. \tag{141}$$

Equation 139b is true because Monin-Obukhov similarity aligns the x axis with the mean wind (the U component) and assumes no turning of the wind in the surface layer.

Likewise, on seeing eq 116 and considering the scales involved, we can show that the profiles in the Ekman layer should obey defect laws (Blackadar and Tennekes 1968; Yamada 1976; Tennekes 1982; Brutsaert 1982, p. 72 ff.) such that

$$\frac{U(z) - \hat{U}}{u_*} = F_U(z/h, h/L) \tag{142a}$$

$$\frac{V(z) - \hat{V}}{u_*} = sgnf\, F_V(z/h, h/L), \tag{142b}$$

$$\frac{\Theta(z) - \hat{\Theta}}{t_*} = F_\Theta(z/h, h/L) \tag{143}$$

$$\frac{Q(z) - \hat{Q}}{q_*} = F_Q(z/h, h/L). \tag{144}$$

In these, $\hat{U}$, $\hat{V}$, $\hat{\Theta}$ and $\hat{Q}$ are, respectively, longitudinal velocity, transverse velocity, potential temperature and specific humidity scales that I will explain shortly.

If the scaling is accurate, the functions F_U, F_V, F_Θ and F_Q should depend only on the dimensionless ratios z/h and h/L, where h is now the height of the ABL and L is again the Obukhov length. In particular, these functions should not depend on the surface Rossby number $G/|f|z_0$ (Blackadar and Tennekes 1968, Tennekes 1973, Hess 1992). Thus, these and subsequent arguments are generally referred to as Rossby number similarity (Blackadar and Tennekes 1968, Hess 1973, Tennekes 1973).

Although to continue the similarity arguments we do not need a formal definition of h, this is a good time to digress on its meaning. As I explained, the presence of turbulence is essential to the definition of the ABL. Consequently, h should denote the surface that separates the turbulent ABL from the (generally) nonturbulent upper air. Rarely, however, do we have profiles of turbulence intensities through the ABL, let alone into the upper air. Thus, it is common to use a surrogate, such as the height of the temperature inversion z_i, as an estimate for h (e.g., Kaimal et al. 1976). While z_i is a good estimate for h in the convective boundary layer, in the stable boundary layer often found over polar marine surfaces, z_i can overestimate h (e.g., Mahrt et al. 1979).

Hanna (1969) reviewed a host of empirical methods for estimating h from surrogate information in both stable and unstable conditions. Mahrt et al. (1979) concentrated on estimating h in the stable ABL. Their main conclusion was that the height of the core of the low-level jet (z_j) that is common in stable boundary layers is a good estimator of h. In turn, the height of the turbulent layer predicted by a Richardson number criterion, z_{Ri}, is well correlated with z_j. Here, a bulk gradient Richardson number is computed from

$$Ri(z) = \frac{g\,z}{\Theta(z)} \frac{\Theta(z) - T_s}{U(z)^2 + V(z)^2} \tag{145}$$

and z_{Ri} is defined as the height at which

$$Ri(z_{Ri}) \geq 0.4 \tag{146}$$

where 0.4 is the critical Richardson number (see also Heinemann and Rose 1990).

On Ice Station Weddell, our radiosondes often found low-level jets (Andreas et al. 1993a, Claffey et al. 1994, Andreas et al. 1995). If we assume, as Mahrt et al. (1979) did, that z_j is an estimate for h, Figure 25 shows that the inversion height is usually a poor estimate of h in the stable ABL. In defining z_i in this figure, we used Kahl's (1990) definition. As such, z_i could be called the top of the inversion layer. In unstable conditions, on the other hand, z_i is often taken as the base of the inversion (e.g., Kaimal et al. 1976). The conflicting definitions arise because in a stable ABL the inversion base is often at the surface (Kahl 1990, Serreze et al. 1992, Claffey et al. 1994).

Figure 26, in contrast, suggests that z_{Ri}, which approximates the height at which turbulence ceases, is a fair estimate of h—if we assume that h corresponds to z_j, the height of the jet core. Thus, we see that over sea ice in late fall and winter, the ABL is generally quite shallow; in Figure 26, z_j is usually between 50 and 300 m. Overland and Guest (1991) and Guest and Davidson (1994) offered additional insight into how the radiation budget, especially during the winter, dictates the thermal and turbulent structure of the ABL and, therefore, its height.

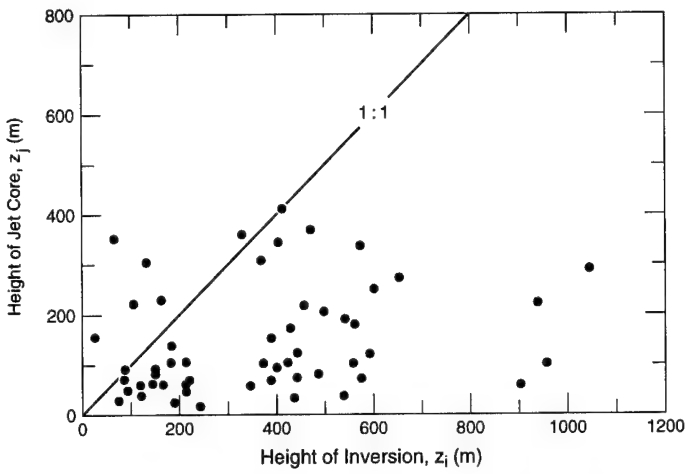

Figure 25. Observations of the height of the core of the low-level jet (z_j) and of the corresponding height of the inversion (z_i) on Ice Station Weddell (Claffey et al. 1994, Andreas et al. 1995).

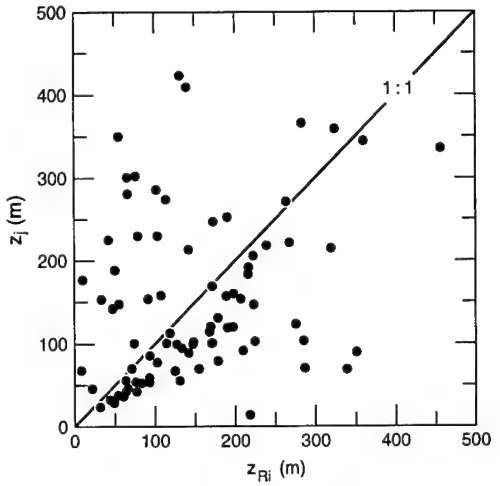

Figure 26. Observations of the height of the jet core (z_j), a surrogate for h, *versus the estimated height of the turbulent layer from a Richardson number criterion (z_{Ri}) (see eq 145 and 146) (Andreas et al. 1995).*

Now back to Rossby number similarity.

Since eq 139–141 and eq 142–144 are two sets of expressions for the same quantities, there should exist a height interval in which both sets are true. That is, as $z/z_0 \to \infty$ (and $z/z_T \to \infty$, $z/z_Q \to \infty$) and as $z/h \to 0$, the two formal descriptions of the atmospheric profiles should be simultaneously accurate (Blackadar and Tennekes 1968, Tennekes 1982, Hess 1992). In these asymptotic limits, eq 139–141 and eq 142–144 require that

$$\frac{U(z)}{u_*} = \frac{1}{k}\left[\ln(z/z_0) - \psi_m(z/L)\right] = F_U(z/h, h/L) + \frac{\hat{U}}{u_*} \tag{147a}$$

$$\frac{V(z)}{u_*} = 0 = sgnf\, F_V(z/h, h/L) + \frac{\hat{V}}{u_*} \tag{147b}$$

$$\frac{\Theta(z)}{t_*} = \frac{1}{k}\left[\ln(z/z_T) - \psi_h(z/L)\right] + \frac{T_s}{t_*} = F_\Theta(z/h, h/L) + \frac{\hat{\Theta}}{t_*} \tag{148}$$

$$\frac{Q(z)}{t_*} = \frac{1}{k}\left[\ln(z/z_Q) - \psi_h(z/L)\right] + \frac{Q_s}{q_*} = F_Q(z/h, h/L) + \frac{\hat{Q}}{q_*}. \tag{149}$$

It is straightforward to rearrange and rewrite eq 147–149 as

$$A(\mu) \equiv \ln(h/z_0) - \frac{k\hat{U}}{u_*} = k\,F_U(z/h, \mu) + \psi_m(\mu) - \ln(z/h) \tag{150a}$$

$$B(\mu) \equiv \frac{-k\hat{V}}{u_*} sgnf = k\,F_V(z/h, \mu) \tag{150b}$$

$$C(\mu) \equiv \ln(h/z_T) + \frac{k\left(T_s - \hat{\Theta}\right)}{t_*} = k\,F_\Theta(z/h, \mu) + \psi_h(\mu) - \ln(z/h) \tag{151}$$

$$D(\mu) \equiv \ln(h/z_Q) + \frac{k\left(Q_s - \hat{Q}\right)}{q_*} = k\,F_Q(z/h, \mu) + \psi_h(\mu) - \ln(z/h). \tag{152}$$

In each of these, the middle term does not depend on z; consequently, although there is a z in the right term, this term must be independent of z also. Likewise, because the right term depends explicitly on the new stability parameter $\mu = h/L$ (first introduced by Kazanski and Monin 1960), the middle term must also. Therefore, Rossby number similarity lets us define the new profile functions A, B, C and D that depend only on μ. These functions are often called resistance laws because they show how the bulk boundary layer parameters $\hat{U}, \hat{V}, \hat{\theta}, T_s, \hat{Q}, Q_s$ and h are related to the surface properties u_*, t_*, q_*, z_0, z_T, z_Q and L. In a way, A, B, C and D are thus comparable to the bulk transfer coefficients C_{Dr}, C_{Hr} and C_{Er}.

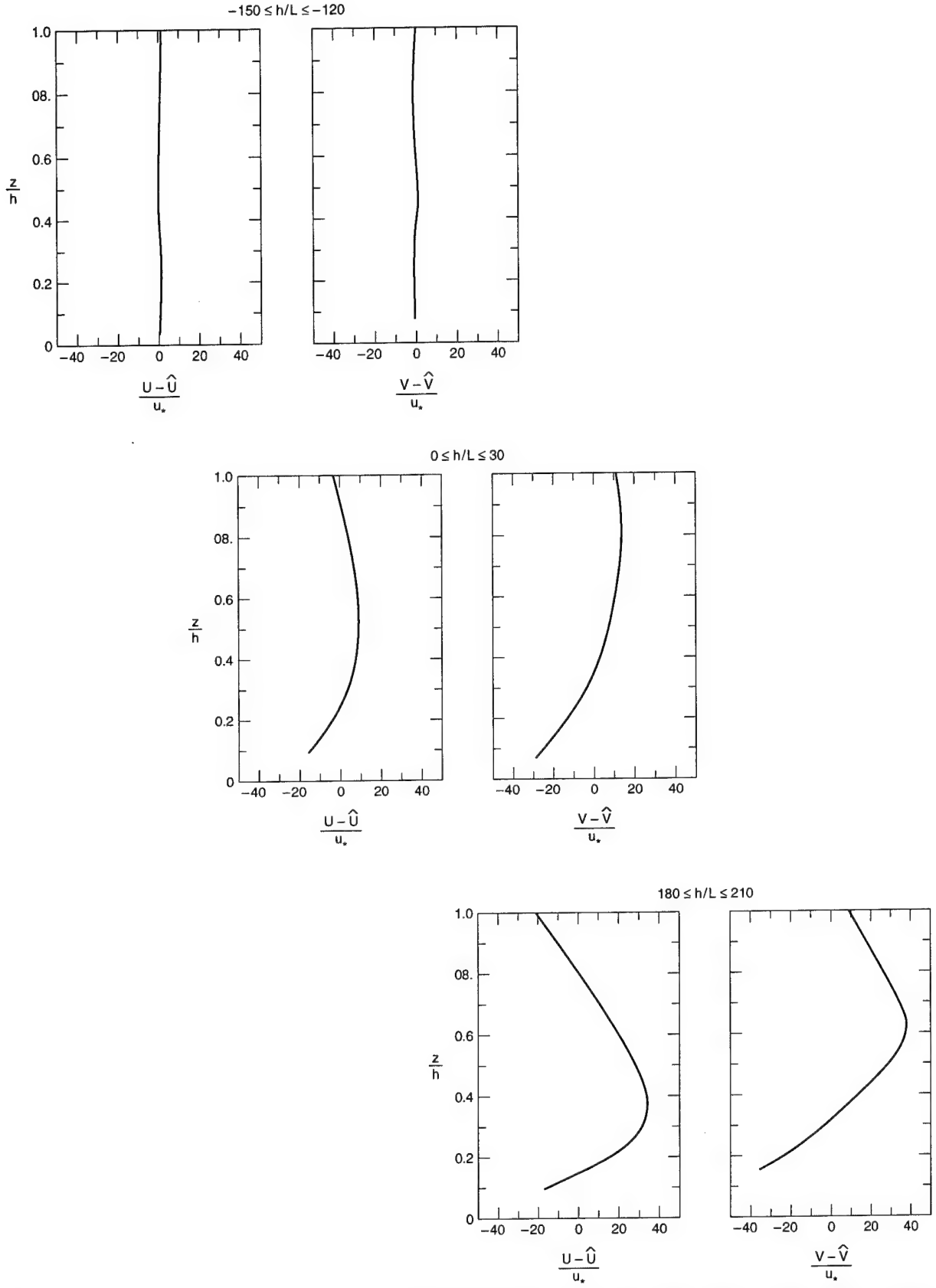

Figure 27. Evaluations of F_U *and* F_V *for very unstable* ($-150 \le \mu \le -120$), *weakly stable* ($0 \le \mu \le 30$), *and very stable* ($180 \le \mu \le 210$) *conditions (after Yamada 1976).*

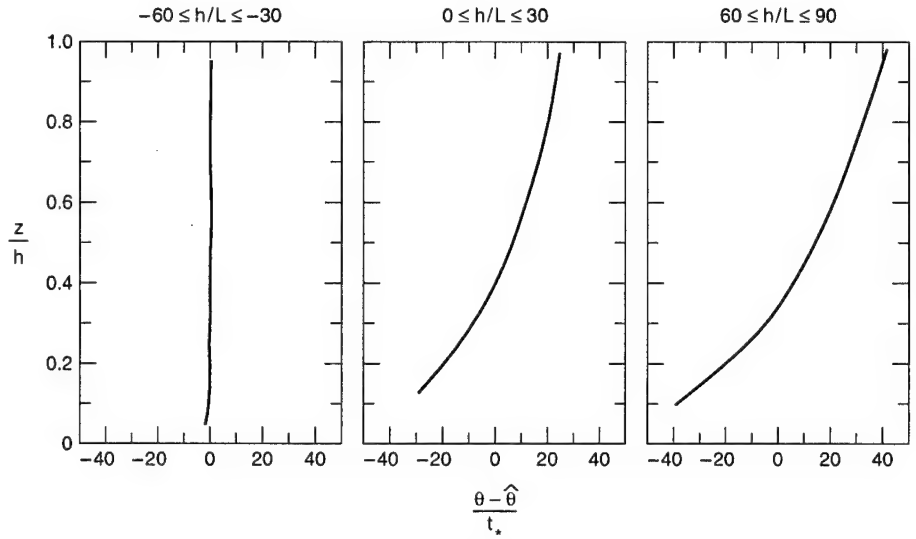

Figure 28. Evaluations of F_Θ *for unstable* ($-60 \le \mu \le -30$), *weakly stable* ($0 \le \mu \le 30$), *and moderately stable* ($60 \le \mu \le 90$) *conditions (after Yamada 1976).*

As with the ϕ_m and ϕ_h or ψ_m and ψ_h functions of Monin-Obukhov similarity, Rossby number similarity essentially leads us on a quest to find the nondimensional, universal functions *A*, *B*, *C* and *D*. Part of this quest requires defining the scales $\hat{U}, \hat{V}, \hat{\Theta}$ and $\hat{Q}$. In analogy with the Ekman equations (i.e., eq 116), we might expect $\hat{U} = U_g, \hat{V} = V_g, \hat{\Theta} = \Theta(h)$ and $\hat{Q} = Q(h)$. But in light of frequent baroclinicity (a thermal wind), Arya and Wyngaard (1975) found that more robust values for $\hat{U}$ and $\hat{V}$ derive from averaging the geostrophic wind from the surface to *h*. Likewise, Yamada (1976) found that $\hat{\Theta}$ is best taken as the height-averaged potential temperature. By extension, I define $\hat{Q}$ analogously. Mathematically, we define

$$\langle \chi \rangle = \frac{1}{h} \int_0^h \chi(z)\, dz \tag{153}$$

where χ is $U(z)$, $V(z)$, $U_g(z)$, $V_g(z)$, $\Theta(z)$ or $Q(z)$. Thus (Arya and Wyngaard 1975, Yamada 1976)

$$\hat{U} = \langle U_g \rangle = \langle U \rangle \tag{154a}$$

$$\hat{V} = \langle V_g \rangle = \langle V \rangle - \frac{u_*^2}{f h} \tag{154b}$$

$$\hat{\Theta} = \langle \Theta \rangle \tag{155}$$

$$\hat{Q} = \langle Q \rangle. \tag{156}$$

After defining $\hat{U}$, $\hat{V}$ and $\hat{\Theta}$ as above, Yamada (1976) made the classic attempt to find F_U, F_V and F_Θ and, thus, *A*, *B* and *C*. Figures 27 and 28 show the F_U, F_V and F_Θ functions that he deduced from plots of data from the Wangara experiment in Hay, Australia. (Brutsaert [1982] offered one of the few discussions of F_Q and *D*.)

Figures 27 and 28 emphasize why it is appropriate to refer to eq 150–152 as resistance laws. These figures show that in very unstable conditions F_U, F_V and F_Θ are all near zero. This means that the ABL is well mixed; the wind vector and temperature at *h* are very near the values at the surface. That is, there is efficient coupling between the upper air and the surface. In very stable conditions, in contrast, $U(z)$, $V(z)$ and $\Theta(z)$ vary strongly with height. In other words, in stable conditions the transfer of properties from the surface to the top of the ABL, or vice versa, is inefficient.

From his analysis, Yamada (1976) was able to estimate *A*, *B* and *C*. Many others since Yamada have suggested alternate formulations (e.g., Arya 1977, Zilitinkevich 1989a, b). I do not have room here to review all of these; thus, since Yamada's functions are the most frequently cited, I will base the remainder of this section on them. He found

$$A(\mu) = 10.0 - 8.145\,(1 - 0.008376\,\mu)^{-1/3} \quad \text{for } \mu \le 0 \tag{157a}$$

$$= 1.855 - 0.380\,\mu \quad \text{for } 0 \le \mu \le 35 \tag{157b}$$

$$= -2.94\,(\mu - 19.94)^{1/2} \quad \text{for } 35 \le \mu \tag{157c}$$

$$B(\mu) = 3.020\,(1 - 3.290\,\mu)^{-1/3} \quad \text{for } \mu \le 0 \tag{158a}$$

$$= 3.020 + 0.300\,\mu \quad \text{for } 0 \le \mu \le 35 \tag{158b}$$

$$= 2.85\,(\mu - 12.47)^{1/2} \quad \text{for } 35 \le \mu \tag{158c}$$

$$C(\mu) = 12.0 - 8.335\,(1.0 - 0.03106\,\mu)^{-1/3} \quad \text{for } \mu \le 0 \tag{159a}$$

$$= 3.665 - 0.829\,\mu \quad \text{for } 0 \le \mu \le 18 \tag{159b}$$

$$= -4.32\,(\mu - 11.21)^{1/2} \quad \text{for } 18 \le \mu\,. \tag{159c}$$

Figure 29 shows plots of these.

other words, the wind vector turns. Likewise, eq 150a and 151 suggest that we cannot easily infer the profiles of $U(z)$ and $\Theta(z)$ higher in the ABL from the values at the top of the surface layer.

Equation 47 defined the geostrophic drag coefficient C_g as u_*/G. To be compatible with the preferred Ekman-layer scales, rather than defining G as in eq 131, here I use

$$G = \left(\hat{U}^2 + \hat{V}^2\right)^{1/2}. \tag{160}$$

Thus, using eq 150, we can express C_g in terms of the A and B functions

$$C_g \equiv \frac{u_*}{G} = \frac{k}{\left\{\left[\ln(h/z_0) - A(\mu)\right]^2 + B(\mu)^2\right\}^{1/2}}. \tag{161}$$

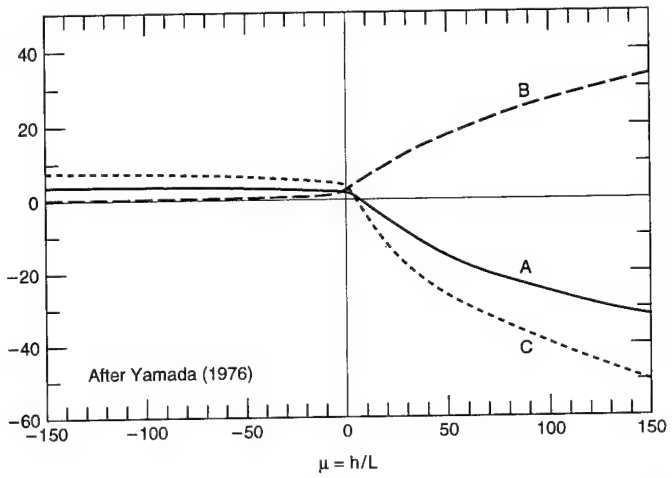

Figure 29. Yamada's (1976) resistance laws for the longitudinal (A) *and transverse* (B) *velocity components and for the potential temperature* (C) *as functions of the stability parameter* μ = h/L *(see eq 157–159).*

Again, we can interpret the behavior of the curves in Figure 29 as an indication of the resistance the ABL offers to the vertical transfer of properties. In unstable conditions ($\mu < 0$), A, B and C are relatively small. From eq 150 and 151 we thus infer that the ABL is well mixed. Equation 150b shows that there is little turning in the wind between the top of the surface layer and the top of the ABL. And eq 150a and 151 show a nearly semi-logarithmic relationship between height and $\hat{U}$ and $\hat{\Theta}$—the same basic relation found in the surface layer. Thus, again, conditions extant at the top of the surface layer continue, with little change, high into the ABL.

In the stable half of Figure 29 ($\mu > 0$), however, we see the opposite behavior. A, B and C deviate increasingly from zero as the stability increases. Equation 150b thus shows that V becomes significant. In

Likewise, eq 133 defined the turning angle α. Our Rossby number similarity solutions, however, provide another definition of α that depends on stability

$$\tan\alpha = \frac{\hat{V}}{\hat{U}} \tag{162}$$

where α is now the turning angle between the surface-layer wind and the vertically integrated geostrophic wind (see eq 154). Again, from eq 150, we can express 162 as

$$\tan\alpha = \frac{-sgnf\,B(\mu)}{\ln(h/z_0) - A(\mu)}. \tag{163}$$

Figure 30 shows plots of C_g and α as functions of stability when Yamada's (1976) functions are used for

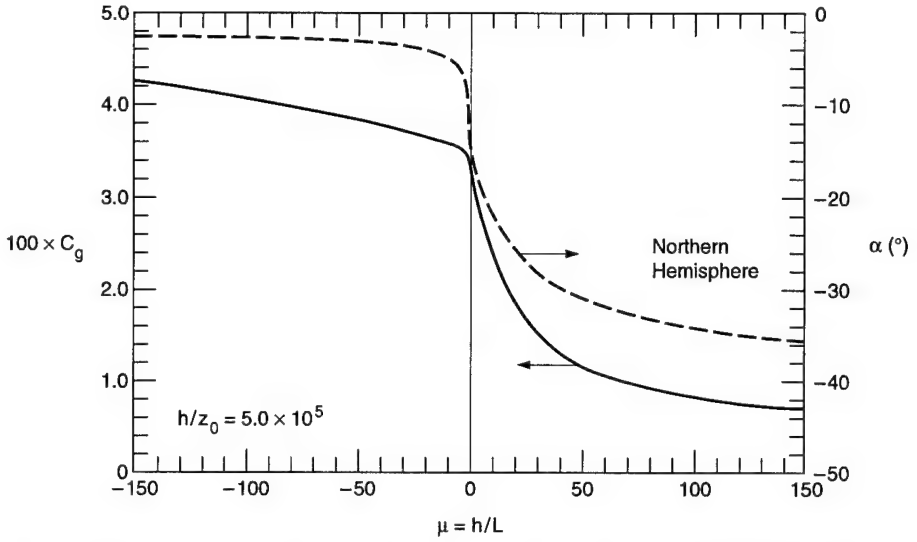

Figure 30. Geostrophic drag coefficient (C_g) *and the turning angle* (α) *as functions of stability when Yamada's (1976)* A *and* B *functions (eq 157–158) are used in eq 161 and 163, respectively. To make this calculation, I used* $h/z_0 = 5.0 \times 10^5$. *The* α *values are for the Northern Hemisphere; Southern Hemisphere values have the opposite sign.*

A and B. This figure again points out the resistance-law interpretation of A and B. In unstable conditions, C_g is large and α is near zero. As a result, the surface stress responds strongly to geostrophic forcing. And because of this strong coupling, the ABL is well mixed so the turning of the wind vector with height is small. On the other hand, in very stable conditions, C_g is smaller and α is larger in magnitude. That is, because the stratification suppresses the vertical turbulent exchange, the surface stress is less responsive to the geostrophic forcing. Also with less efficient vertical coupling, the wind vector can rotate more with height because the upper-level winds have little opportunity to mix their longitudinal momentum down into the ABL.

Brown (1981, 1990), Overland and Davidson (1992) and Overland and Colony (1994) showed some alternative formulations for C_g and α over sea ice and also presented C_g and α data that came from Arctic sea ice regions. Although their data and the computed parameters in Figure 30 may differ in detail, the trends and the general magnitudes of the quantities agree.

As we did in the atmospheric surface layer, we can also write an expression for the geostrophic drag coefficient at neutral stability. From eq 161, this is

$$C_{gN} = \frac{k}{\left\{\left[\ln(h/z_0) - A(0)\right]^2 + B(0)^2\right\}^{1/2}}. \qquad (164)$$

Yamada's (1976) functions (eq 157–158) suggest that $A(0) = 1.855$ and $B(0) = 3.020$. For comparison, Zilitinkevich (1989b) recommended $A(0) = 1.7$ and $B(0) = 4.5$ after an extensive review.

Earlier, I showed that the surface-layer neutral-stability drag coefficient at 10 m (C_{DN10}) is monotonically related to z_0. We can use that relation, eq 105, here to relate C_{gN} and C_{DN10}. Equation 164 thus becomes

$$C_{gN} = \frac{k}{\left\{\left[k\,C_{DN10}^{-1/2} + \ln(h/10) - A(0)\right]^2 + B(0)^2\right\}^{1/2}} \qquad (165)$$

where h must be in meters.

We see two effects here. As C_{DN10} increases, so does C_{gN}. But as the ABL gets deeper (i.e., as h increases), C_{gN} decreases if C_{DN10} remains constant. This latter effect is analogous to what we see in the surface-layer bulk-transfer coefficients. Equations 105–107 show that C_{DNr}, C_{HNr} and C_{ENr} all decrease as the reference height r increases. The reason is that the forcing quantities $U_r - 0$, $T_s - \Theta_r$ and $Q_s - Q_r$ (see eq 91–93) all increase in magnitude with r; thus, the corresponding transfer coefficient can decrease proportionately.

From eq 164 we can also solve for z_0 in terms of C_{gN}

$$z_{0_{ef}} = h\exp\left\{-\left[A(0) + \left((k/C_{gN})^2 - B(0)^2\right)^{1/2}\right]\right\}. \qquad (166)$$

Since this roughness length derives from Ekman layer parameters, it is the effective roughness length (Fiedler and Panofsky 1972, Arya 1975, Mason 1988, Claussen 1990) in contrast to the local roughness length, which

is the correct surface-layer interpretation of z_0. Thus, we see that—as in the surface layer—finding the geostrophic drag coefficient at neutral stability is tantamount to finding the effective roughness length, and vice versa.

SUMMARY

Several good problems in the atmospheric boundary layer over sea ice still exist. I have highlighted a few of these. One is to investigate turbulent exchange and the turbulence statistics in the atmospheric surface layer in stable conditions. A related study is to narrow the uncertainty in the nondimensional gradient functions, ϕ_m and ϕ_h, for stable conditions (see Fig. 5). Efforts here would benefit not only polar scientists but boundary-layer meteorologists everywhere. The stable boundary layer is seldom in quasi-steady-state at lower latitudes; consequently, obtaining robust statistics in stable stratification is more difficult here than it is in the polar regions.

Another good problem is to devise a new parameterization for C_{DN10} in terms of some measurable surface properties that—preferably—can be sensed remotely. The relation from Banke et al. (1980) (eq 111) is quite suggestive but evidently impractical in light of my recent work on how drifting snow can rapidly alter C_{DN10}.

A related issue is obtaining good measurements of C_{HN10} and C_{EN10} over sea ice. These are conspicuous by their absence from the literature. The primary reason for the scanty number of observations is that the forcing terms $T_s - \Theta_r$ and $Q_s - Q_r$ necessary to compute C_{HNr} and C_{ENr} are small over sea ice and notoriously difficult to measure. It may, thus, be time to revise our typical measurement practices or to rethink the entire method of parameterizing sensible and latent heat fluxes over sea ice in terms of bulk transfer coefficients.

Because the geostrophic drag coefficient is related monotonically to the effective roughness length $z_{0_{ef}}$, it should be possible to bootstrap information about geostrophic drag from the many observations of z_0 and C_{DN10} over sea ice. The key step is inferring $z_{0_{ef}}$ from z_0. Several have thought about this problem, but, to my knowledge, only Arya (1975) has attempted to include the unique topographic features of sea ice in the transformation. In light of the recent flurry of papers on area averaging (e.g., Mason 1988; Claussen 1990, 1991; Vihma and Savijärvi 1991; Blyth et al. 1993; Moore et al. 1993), this problem might be ripe for a productive revisit.

LITERATURE CITED

Anderson, R.J. (1987) Wind stress measurements over rough ice during the 1984 Marginal Ice Zone Experiment. *Journal of Geophysical Research*, **92**: 6933–6941.

Andreas, E.L (1987) A theory for the scalar roughness and the scalar transfer coefficients over snow and sea ice. *Boundary-Layer Meteorology*, **38**: 159–184.

Andreas, E.L (1988) Estimating averaging times for point and path-averaged measurements of turbulence spectra. *Journal of Applied Meteorology*, **27**: 295–304.

Andreas, E.L (1995a) Air-ice drag coefficients in the western Weddell Sea: 2. A model based on form drag and drifting snow. *Journal of Geophysical Research*, **100:** 4833–4843.

Andreas, E.L (1995b) A physically based model of the form drag associated with sastrugi. USA Cold Regions Research and Engineering Laboratory, CRREL Report 95-16.

Andreas, E.L and K.J. Claffey (1995) Air-ice drag coefficients in the western Weddell Sea: 1. Values deduced from profile measurements. *Journal of Geophysical Research,* **100:** 4821–4831.

Andreas, E.L and B. Murphy (1986) Bulk transfer coefficients for heat and momentum over leads and polynyas. *Journal of Physical Oceanography*, **16**: 1875–1883.

Andreas, E.L, W.B. Tucker III and S.F. Ackley (1984) Atmospheric boundary-layer modification, drag coefficient and surface heat flux in the Antarctic marginal ice zone. *Journal of Geophysical Research*, **89**: 649–661.

Andreas, E.L, K.J. Claffey and A.P. Makshtas (1993a) Low-level jets and inversions on Ice Station Weddell 1. *Antarctic Journal of the United States*, **28**(5): 274–276.

Andreas, E.L, M.A. Lange, S.F. Ackley and P. Wadhams (1993b) Roughness of Weddell Sea ice and estimates of the air-ice drag coefficient. *Journal of Geophysical Research*, **98**: 12,439–12,452.

Andreas, E.L, K.J. Claffey and A.P. Makshtas (1995) Low-level atmospheric jets over the western Weddell Sea. In *Preprint Volume, Fourth Conference on Polar Meteorology and Oceanography, Dallas, Texas, 15–20 January 1995*. American Meteorological Society, Boston, p. 252–257.

Anonymous (1992) U.S. and Russian scientists complete historic Weddell Sea investigation. *Antarctic Journal of the United States*, **27**(4): 8–11.

Arya, S.P.S. (1973) Contribution of form drag on pressure ridges to the air stress on Arctic ice. *Journal of Geophysical Research*, **78**: 7092–7099.

Arya, S.P.S. (1975) A drag partition theory for determining the large-scale roughness parameter and wind stress on the Arctic pack ice. *Journal of Geophysical Research*, **80**: 3447–3454.

Arya, S.P.S. (1977) Suggested revisions to certain boundary layer parameterization schemes used in atmospheric circulation models. *Monthly Weather Review*, **105**: 215–227.

Arya, S.P.S. (1988) *Introduction to Micrometeorology*. San Diego: Academic Press.

Arya, S.P.S. and J.C. Wyngaard (1975) Effect of baroclinicity on wind profiles and the geostrophic drag law for the convective planetary boundary layer. *Journal of the Atmospheric Sciences*, **32**: 767–778.

Augstein, E., N. Bagriantsev and H.W. Schenke (1991) The expedition ANTARKTIS VIII/1–2, 1989 with the Winter Weddell Gyre Study of the research vessels "*Polarstern*" and "*Akademic Fedorov*." *Berichte zur Polarforschung*, **84**: 1–129.

Banke, E.G., S.D. Smith and R.J. Anderson (1980) Drag coefficients at AIDJEX from sonic anemometer measurements. In *Sea Ice Processes and Models* (R.S. Pritchard, Ed.). Seattle: University of Washington Press, p. 430–442.

Barry, P.J. and R.E. Munn (1967) Use of radioactive tracers in studying mass transfer in the atmospheric boundary layer. *Physics of Fluids*, **10**: 5263–5266.

Beljaars, A.C.M. and A.A.M. Holtslag (1991) Flux parameterization over land surfaces for atmospheric models. *Journal of Applied Meteorology*, **30**: 327–341.

Blackadar, A.K. (1963) The vertical distribution of wind in a baroclinic adiabatic atmospheric boundary layer. Presented at 211th national meeting of the American Meteorological Society, 21–24 January 1963, New York, N.Y. (*Bulletin of the American Meteorological Society*, **43**: 661–674.)

Blackadar, A.K. and H. Tennekes (1968) Asymptotic similarity in neutral barotropic planetary boundary layers. *Journal of the Atmospheric Sciences*, **25**: 1015–1020.

Blyth, E.M., A.J. Dolman and N. Wood (1993) Effective resistance to sensible- and latent-heat flux in heterogeneous terrain. *Quarterly Journal of the Royal Meteorological Society*, **119**: 423–442.

Brown, R.A. (1974) *Analytical Methods in Planetary Boundary Layer Modelling*. New York: John Wiley and Sons.

Brown, R.A. (1981) Modeling the geostrophic drag coefficient for AIDJEX. *Journal of Geophysical Research*, **86**: 1989–1994.

Brown, R.A. (1986) The planetary boundary layer in the marginal ice zone. *MIZEX Bulletin VII*, p. 41–54. (USA Cold Regions Research and Engineering Laboratory, Special Report 86-3.)

Brown, R.A. (1990) Meteorology. In *Polar Oceanography* (W.O. Smith, Jr., Ed.). San Diego: Academic Press, p. 1–46.

Brutsaert, W. (1975a) A theory for local evaporation (or heat transfer) from rough and smooth surfaces at ground level. *Water Resources Research*, **11**: 543–550.

Brutsaert, W. (1975b) The roughness length for water vapor, sensible heat and other scalars. *Journal of the Atmospheric Sciences*, **32**: 2028–2031.

Brutsaert, W.H. (1982) *Evaporation into the Atmosphere: Theory, History and Applications*. Dordrecht: D. Reidel.

Busch, N.E. (1973) On the mechanics of atmospheric turbulence. In *Workshop on Micrometeorology* (D.A. Haugen, Ed.). Boston: American Meteorological Society, p. 1–65.

Businger, J.A. (1966) Transfer of momentum and heat in the planetary boundary layer. In *Proceedings of the Symposium on the Arctic Heat Budget and Atmospheric Circulation* (J.O. Fletcher, Ed.). Santa Monica, California: Rand Corporation, RM–5233-NSF, p. 305–332.

Businger, J.A. (1973) Turbulent transfer in the atmospheric surface layer. In *Workshop on Micrometeorology* (D.A. Haugen, Ed.). Boston: American Meteorological Society, p. 67–100.

Businger, J.A. (1982) Equations and concepts. In *Atmospheric Turbulence and Air Pollution Modelling* (F.T.M. Nieuwstadt and H. van Dop, Ed.). Dordrecht: D. Reidel, p. 1–36.

Businger, J.A. (1988) A note on the Businger-Dyer profiles. *Boundary-Layer Meteorology*, **42**: 145–151.

Businger, J.A. and A.M. Yaglom (1971) Introduction to Obukhov's paper on "Turbulence in an atmosphere with a non-uniform temperature." *Boundary-Layer Meteorology*, **2**: 3–6.

Businger, J.A., J.C. Wyngaard, Y. Izumi and E.F. Bradley (1971) Flux-profile relationships in the atmospheric surface layer. *Journal of the Atmospheric Sciences*, **28**: 181–189.

Claffey, K.J., E.L Andreas and A.P. Makshtas (1994) Upper-air data collected on Ice Station Weddell. USA Cold Regions Research and Engineering Laboratory, Special Report 94-25.

Claussen, M. (1990) Area-averaging of surface fluxes in a neutrally stratified, horizontally inhomogeneous atmospheric boundary layer. *Atmospheric Environment*, **24A**: 1349–1360.

Claussen, M. (1991) Estimation of areally-averaged surface fluxes. *Boundary-Layer Meteorology*, **54**: 387–410.

Deardorff, J.W. (1968) Dependence of air-sea transfer coefficients on bulk stability. *Journal of Geophysical Research*, **73**: 2549–2557.

Dyer, A.J. (1974) A review of flux-profile relationships. *Boundary-Layer Meteorology*, **7**: 363–372.

Dyer, A.J. and E.F. Bradley (1982) An alternative analysis of flux-gradient relationships at the 1976 ITCE. *Boundary-Layer Meteorology*, **22**: 3–19.

Dyer, A.J. and B.B. Hicks (1970) Flux-gradient relationships in the constant flux layer. *Quarterly Journal of the Royal Meteorological Society*, **96**: 715–721.

Ekman, V.W. (1905) On the influence of the Earth's rotation on ocean-currents. *Arkiv für Matematik, Astronomi och Fysik*, **2**: 1–53.

Fairall, C.W. and S.E. Larsen (1986) Inertial-dissipation

methods and turbulent fluxes at the air/ocean interface. *Boundary-Layer Meteorology*, **34**: 287–301.

Fairall, C.W. and R. Markson (1987) Mesoscale variations in surface stress, heat fluxes and drag coefficient in the marginal ice zone during the 1983 Marginal Ice Zone Experiment. *Journal of Geophysical Research*, **92**: 6921–6932.

Fiedler, F. and H.A. Panofsky (1972) The geostrophic drag coefficient and the 'effective' roughness length. *Quarterly Journal of the Royal Meteorological Society*, **98**: 213–220.

Garratt, J.R. (1992) *The Atmospheric Boundary Layer.* Cambridge, England: Cambridge University Press.

Guest, P.S. and K.L. Davidson (1987) The effect of observed ice conditions on the drag coefficient in the summer East Greenland Sea marginal ice zone. *Journal of Geophysical Research*, **92**: 6943–6954.

Guest, P.S. and K.L. Davidson (1991) The aerodynamic roughness of different types of sea ice. *Journal of Geophysical Research*, **96**: 4709–4721.

Guest, P.S. and K.L. Davidson (1994) Factors affecting variations of snow surface temperature and air temperature over sea ice in winter. In *The Polar Oceans and Their Role in Shaping the Global Environment* (O.M. Johannessen, R.D. Muench and J.E. Overland, Ed.). Washington, D.C.: American Geophysical Union, p. 435–442.

Hanna, S.R. (1969) The thickness of the planetary boundary layer. *Atmospheric Environment*, **3**: 519–536.

Harr, M.E. (1977) *Mechanics of Particulate Media: A Probabilistic Approach.* New York: McGraw-Hill.

Haugen, D.A. (Ed.) (1973) *Workshop on Micrometeorology.* Boston: American Meteorological Society.

Haugen, D.A., J.C. Kaimal and E.F. Bradley (1971) An experimental study of Reynolds stress and heat flux in the atmospheric surface layer. *Quarterly Journal of the Royal Meteorological Society*, **97**: 168–180.

Heinemann, G. and L. Rose (1990) Surface energy balance, parameterizations of boundary-layer heights and the application of resistance laws near an Antarctic ice shelf front. *Boundary-Layer Meteorology*, **51**: 123–158.

Hess, G.D. (1973) On Rossby-number similarity theory for a baroclinic planetary boundary layer. *Journal of the Atmospheric Sciences*, **30**: 1722–1723.

Hess, G.D. (1992) Observations and scaling of the atmospheric boundary layer. *Australian Meteorological Magazine*, **41**: 79–99.

Hibler, W.D. III (1979) A dynamic thermodynamic sea ice model. *Journal of Physical Oceanography*, **9**: 815–846.

Hicks, B.B. (1976) Wind profile relationships from the 'Wangara' experiment. *Quarterly Journal of the Royal Meteorological Society*, **102**: 535–551.

Hicks, B.B. and H.C. Martin (1972) Atmospheric turbulent fluxes over snow. *Boundary-Layer Meteorology*, **2**: 496–502.

Hill, R.J. (1989) Implications of Monin-Obukhov similarity theory for scalar quantities. *Journal of the Atmospheric Sciences*, **46**: 2236–2244.

Hinze, J.O. (1975) *Turbulence.* New York: McGraw-Hill, 2nd edition.

Högström, U. (1988) Non-dimensional wind and temperature profiles in the atmospheric surface layer: A re-evaluation. *Boundary-Layer Meteorology*, **42**: 55–78.

Holtslag, A.A.M. and H.A.R. de Bruin (1988) Applied modeling of the nighttime surface energy balance over land. *Journal of Applied Meteorology*, **27**: 689–704.

Inoue, J. (1989) Surface drag over the snow surface of the Antarctic Plateau: 1. Factors controlling surface drag over the katabatic wind region. *Journal of Geophysical Research*, **94**: 2207–2217.

ISW Group (1993) Weddell Sea exploration from ice station. *Eos, Transactions of the American Geophysical Union*, **74**: 121–126.

Jackson, B.S. and J.J. Carroll (1978) Aerodynamic roughness as a function of wind direction over asymmetric surface elements. *Boundary-Layer Meteorology*, **14**: 323–330.

Joffre, S.M. (1982) Momentum and heat transfers in the surface layer over a frozen sea. *Boundary-Layer Meteorology*, **24**: 211–229.

Kahl, J.D. (1990) Characteristics of the low-level temperature inversion along the Alaskan coast. *International Journal of Climatology*, **10**: 537–548.

Kaimal, J.C. and J.J. Finnigan (1994) *Atmospheric Boundary Layer Flows: Their Structure and Measurement.* New York: Oxford University Press.

Kaimal, J.C., J.C. Wyngaard, D.A. Haugen, O.R. Coté, Y. Izumi, S.J. Caughey and C.J. Readings (1976) Turbulence structure in the convective boundary layer. *Journal of the Atmospheric Sciences*, **33**: 2152–2169.

Kazanski, A.B. and A.S. Monin (1960) A turbulent regime above the ground atmospheric layer. *Izvestiya, Geophysical Series,* no. 1, p. 110–112.

Kondo, J. and H. Yamazawa (1986) Bulk transfer coefficient over a snow surface. *Boundary-Layer Meteorology*, **34**: 123–135.

Lange, M.A. and H. Eichen (1991) The sea ice thickness distribution in the northwestern Weddell Sea. *Journal of Geophysical Research*, **96**: 4821–4837.

Large, W.G. and S. Pond (1981) Open ocean momentum flux measurements in moderate to strong winds. *Journal of Physical Oceanography*, **11**: 324–336.

Large, W.G. and S. Pond (1982) Sensible and latent heat flux measurements over the ocean. *Journal of Physical Oceanography*, **12**: 464–482.

Launiainen, J. and T. Vihma (1990) Derivation of turbulent surface fluxes—An iterative flux-profile method allowing arbitrary observing heights. *Environmental Software*, **5**: 113–124.

Lettau, H.H. (1979) Wind and temperature profile pre-

diction for diabatic surface layers including strong inversion cases. *Boundary-Layer Meteorology*, **17**: 443–464.
Lumley, J.L. and H.A. Panofsky (1964) *The Structure of Atmospheric Turbulence*. New York: Interscience.
Lytle, V.I. and S.F. Ackley (1991) Sea ice ridging in the eastern Weddell Sea. *Journal of Geophysical Research*, **96**: 18,411–18,416.
Mahrt, L. (1981) Modeling the depth of the stable boundary-layer. *Boundary-Layer Meteorology*, **21**: 3–19.
Mahrt, L., R.C. Heald, D.H. Lenschow, B.B. Stankov and I. Troen (1979) An observational study of the structure of the nocturnal boundary layer. *Boundary-Layer Meteorology*, **17**: 247–264.
Makshtas, A.P. (1991) *The Heat Budget of Arctic Ice in the Winter.* Cambridge, England: International Glaciological Society.
Martinson, D.G. and C. Wamser (1990) Ice drift and momentum exchange in winter Antarctic pack ice. *Journal of Geophysical Research*, **95**: 1741–1755.
Mason, P.J. (1988) The formation of areally-averaged roughness lengths. *Quarterly Journal of the Royal Meteorological Society*, **114**: 399–420.
Maykut, G.A. (1978) Energy exchange over young sea ice in the central Arctic. *Journal of Geophysical Research*, **83**: 3646–3658.
McPhee, M.G. and D.G. Martinson (1994) Turbulent mixing under drifting pack ice in the Weddell Sea. *Science*, **263**: 218–221.
Monin, A.S. and A.M. Obukhov (1954) Basic laws of turbulent mixing in the ground layer of the atmosphere (in Russian). *Trudy, Akademiia Nauk SSSR, Geofizicheskii Instituta*, **24**: 163–187.
Monin, A.S. and A.M. Yaglom (1971) *Statistical Fluid Mechanics: Mechanics of Turbulence.* Cambridge, Massachusetts: MIT Press, vol. 1.
Moore, K.E., D.R. Fitzjarrald and J.A. Ritter (1993) How well can regional fluxes be derived from smaller-scale estimates? *Journal of Geophysical Research*, **98**: 7187–7198.
Morris, E.M. (1989) Turbulent transfer over snow and ice. *Journal of Hydrology*, **105**: 205–223.
Munro, D.S. (1989) Surface roughness and bulk heat transfer on a glacier: Comparison with eddy correlation. *Journal of Glaciology*, **35**: 343–348.
Nansen, F. (1897) *Farthest North.* New York: Harper and Brothers, vol. I and II.
National Weather Service (1991) Observing Handbook No. 1: Marine Surface Weather Observations. Silver Spring, Maryland: U.S. Department of Commerce, National Oceanic and Atmospheric Administration.
Obukhov, A.M. (1971) Turbulence in an atmosphere with a non-uniform temperature. *Boundary-Layer Meteorology*, **2**: 7–29.
Overland, J.E. (1985) Atmospheric boundary layer structure and drag coefficients over sea ice. *Journal of Geophysical Research*, **90**: 9029–9049.
Overland, J.E. and R.L. Colony (1994) Geostrophic drag coefficients for the central Arctic derived from Soviet drifting station data. *Tellus*, **46A**: 75–85.
Overland, J.E. and K.L. Davidson (1992) Geostrophic drag coefficients over sea ice. *Tellus*, **44**: 54–66.
Overland, J.E. and P.S. Guest (1991) The Arctic snow and air temperature budget over sea ice during winter. *Journal of Geophysical Research*, **96**: 4651–4662.
Panofsky, H.A. (1963) Determination of stress from wind and temperature measurements. *Quarterly Journal of the Royal Meteorological Society*, **89**: 85–94.
Panofsky, H.A. and J.A. Dutton (1984) *Atmospheric Turbulence: Models and Methods for Engineering Applications.* New York: John Wiley and Sons.
Parkinson, C.L. and W.M. Washington (1979) A large-scale numerical model of sea ice. *Journal of Geophysical Research*, **84**: 311–337.
Paulson, C.A. (1970) The mathematical representation of wind speed and temperature profiles in the unstable atmospheric surface layer. *Journal of Applied Meteorology*, **9**: 857–861.
Pielke, R.A. (1984) *Mesoscale Meteorological Modeling*. Orlando, Florida: Academic Press.
Plate, E.J. (1971) *Aerodynamic Characteristics of Atmospheric Boundary Layers*. Oak Ridge, Tennessee: U.S. Atomic Energy Commission.
Raupach, M.R. (1992) Drag and drag partition on rough surfaces. *Boundary-Layer Meteorology*, **60**: 375–395.
Schlichting, H. (1968) *Boundary-Layer Theory.* New York: McGraw-Hill, 6th edition.
Serreze, M.C., J.D. Kahl and R.C. Schnell (1992) Low-level temperature inversions of the Eurasian Arctic and comparisons with Soviet drifting station data. *Journal of Climate*, **5**: 615–629.
Shirasawa, K. (1981) Studies on wind stress on sea ice (In Japanese, English summary). *Low Temperature Science*, Ser. A, **40**: 101–118.
Smith, S.D. (1988) Coefficients for sea surface wind stress, heat flux, and wind profiles as a function of wind speed and temperature. *Journal of Geophysical Research*, **93**: 15,467–15,472.
Sorbjan, Z. (1989) *Structure of the Atmospheric Boundary Layer.* Englewood Cliffs, New Jersey: Prentice Hall.
Stull, R.B. (1988) *An Introduction to Boundary Layer Meteorology*. Dordrecht: Kluwer.
Tennekes, H. (1973) Similarity laws and scale relations in planetary boundary layers. In *Workshop on Micrometeorology* (D.A. Haugen, Ed.). Boston: American Meteorological Society, p. 177–216.
Tennekes, H. (1982) Similarity relations, scaling laws and spectral dynamics. In *Turbulence and Air Pollution Modelling* (F.T.M. Nieuwstadt and H. van Dop, Ed.). Dordrecht: D. Reidel, p. 37–68.
Tennekes, H. and J.L. Lumley (1972) *A First Course in*

Turbulence. Cambridge, Massachusetts: MIT Press.

Thorpe, M.R., E.G. Banke and S.D. Smith (1973) Eddy correlation measurements of evaporation and sensible heat flux over Arctic sea ice. *Journal of Geophysical Research*, **78**: 3573–3584.

Vihma, T. and H. Savijärvi (1991) On the effective roughness length for heterogeneous terrain. *Quarterly Journal of the Royal Meteorological Society*, **117**: 399–407.

Viswanadham, Y. (1979) Relation of Richardson number to the curvature of the wind profile. *Boundary-Layer Meteorology*, **17**: 537–544.

Viswanadham, Y. (1982) Examination of the empirical flux-profile models in the atmospheric surface boundary layer. *Boundary-Layer Meteorology*, **22**: 61–77.

Wamser, C. and D.G. Martinson (1993) Drag coefficients for winter Antarctic pack ice. *Journal of Geophysical Research*, **98**: 12,431–12,437.

Webb, E.K. (1970) Profile relationships: The log-linear range and extension to strong stability. *Quarterly Journal of the Royal Meteorological Society*, **96**: 67–90.

Wieringa, J. (1980) A revaluation of the Kansas mast influence on measurements of stress and cup anemometer overspeeding. *Boundary-Layer Meteorology*, **18**: 411–430.

Woods, J.D. (1969) On Richardson's number as a criterion for laminar-turbulent-laminar transition in the ocean and atmosphere. *Radio Science*, **4**: 1289–1298.

Wyngaard, J.C. (1973) On surface-layer turbulence. In *Workshop on Micrometeorology* (D.A. Haugen, Ed.). Boston: American Meteorological Society, p. 101–149.

Wyngaard, J.C. (1992) Atmospheric turbulence. *Annual Review of Fluid Mechanics*, **24**: 205–233.

Yaglom, A.M. (1977) Comments on wind and temperature flux-profile relationships. *Boundary-Layer Meteorology*, **11**: 89–102.

Yamada, T. (1976) On the similarity functions A, B and C of the planetary boundary layer. *Journal of the Atmospheric Sciences*, **33**: 781–793.

Zilitinkevich, S.S. (1966) Effect of humidity stratification on hydrostatic stability. *Akademiia Nauk SSSR, Atmospheric and Oceanic Physics*, **2**: 655–658.

Zilitinkevich, S.S. (1989a) Velocity profiles, the resistance law and the dissipation rate of mean flow kinetic energy in a neutrally and stably stratified planetary boundary layer. *Boundary-Layer Meteorology*, **46**: 367–387.

Zilitinkevich, S.S. (1989b) The temperature profile and heat transfer law in a neutrally and stably stratified planetary boundary layer. *Boundary-Layer Meteorology*, **49**: 1–5.

REPORT DOCUMENTATION PAGE

Form Approved
OMB No. 0704-0188

1. AGENCY USE ONLY (Leave blank)	2. REPORT DATE	3. REPORT TYPE AND DATES COVERED
	June 1996	

4. TITLE AND SUBTITLE

The Atmospheric Boundary Layer Over Polar Marine Surfaces

5. FUNDING NUMBERS

6. AUTHORS

Edgar L Andreas

7. PERFORMING ORGANIZATION NAME(S) AND ADDRESS(ES)

U.S. Army Cold Regions Research and Engineering Laboratory
72 Lyme Road
Hanover, New Hampshire 03755-1290

8. PERFORMING ORGANIZATION REPORT NUMBER

Monograph 96-2

9. SPONSORING/MONITORING AGENCY NAME(S) AND ADDRESS(ES)

National Science Foundation
Arlington, Virginia 22230

and

Office of the Chief of Engineers
Washington, DC 20314-1000

10. SPONSORING/MONITORING AGENCY REPORT NUMBER

11. SUPPLEMENTARY NOTES

12a. DISTRIBUTION/AVAILABILITY STATEMENT

Approved for public release; distribution is unlimited.

Available from NTIS, Springfield, Virginia 22161.

12b. DISTRIBUTION CODE

13. ABSTRACT (*Maximum 200 words*)

The Atmospheric Boundary Layer (ABL) over polar marine surfaces is, in ways, simpler and, in other ways, more complex than ABLs in other environments. It is simpler because topographic effects are rarely a concern, the surface is fairly homogeneous, and roughness lengths over sea ice and the ocean are much smaller than they are over land. It is complex because the stratification is usually stable, and stable ABLs have not yielded to quantification as readily as convective ABLs have. This report reviews some of these characteristics of ABLs over polar marine surfaces. The ABL, by definition, is the turbulent layer between the Earth's surface and the (generally) nonturbulent free atmosphere. Hence, the emphasis is on turbulence processes—in particular, the turbulent transfer of momentum and sensible and latent heat over sea ice. As such, this report reviews both the theoretical and observational bases for our understanding of the mean structure of the ABL. Understanding this structure then allows predicting the turbulent surface fluxes of momentum and sensible and latent heat.

14. SUBJECT TERMS

Air–sea–ice interactions; Atmospheric boundary layer; Cold regions; Polar marine surfaces; Polar meteorology; Turbulence

15. NUMBER OF PAGES
45

16. PRICE CODE

17. SECURITY CLASSIFICATION OF REPORT	18. SECURITY CLASSIFICATION OF THIS PAGE	19. SECURITY CLASSIFICATION OF ABSTRACT	20. LIMITATION OF ABSTRACT
UNCLASSIFIED	UNCLASSIFIED	UNCLASSIFIED	UL